Modelling transmission and control of the COVID-19 pandemic in Australia

Sheryl L. Chang[1], Nathan Harding[1], Cameron Zachreson[1], Oliver M. Cliff[1], and Mikhail Prokopenko[1,2,*]

[1] *Centre for Complex Systems, Faculty of Engineering, University of Sydney, Sydney, NSW 2006, Australia*
[2] *Marie Bashir Institute for Infectious Diseases and Biosecurity, University of Sydney, Westmead, NSW 2145, Australia*
[*] *Corresponding author: mikhail.prokopenko@sydney.edu.au (ORCID: 0000-0002-4215-0344)*

Abstract

We develop an agent-based model for a fine-grained computational simulation of the ongoing COVID-19 pandemic in Australia. This model is calibrated to reproduce key characteristics of COVID-19 transmission. An important calibration outcome is the age-dependent fraction of symptomatic cases, with this fraction for children found to be one-fifth of such fraction for adults. We apply the model to compare several intervention strategies, including restrictions on international air travel, case isolation, home quarantine, social distancing with varying levels of compliance, and school closures. School closures are not found to bring decisive benefits, unless coupled with high level of social distancing compliance. We report several trade-offs, and an important transition across the levels of social distancing compliance, in the range between 70% and 80% levels, with compliance at the 90% level found to control the disease within 13–14 weeks, when coupled with effective case isolation and international travel restrictions.

Key words: `COVID-19, coronavirus, SARS-CoV-2, epidemics, pandemics, interventions, social distancing, mitigation, suppression, computational epidemiology, agent-based modelling`

arXiv:2003.10218v3 [q-bio.PE] 3 May 2020

1. Introduction

The 2019-2020 coronavirus pandemic is an ongoing pandemic of coronavirus disease 2019 (COVID-19), caused by Severe Acute Respiratory Syndrome Coronavirus 2 (SARS-CoV-2). The first outbreak, which originated in December 2019 in Wuhan, the capital of Hubei province, and rapidly spread to the rest of Hubei and all other provinces in China, has been largely eradicated within mainland China by mid- to late March 2020, having generated more than 81,000 cases (cumulative incidence on 20 March 2020 [1]). This was largely due to intense quarantine and social distancing measures, including isolation of detected cases, tracing and management of their close contacts, closures of potential zoonotic sources of SARS-CoV-2, strict traffic restrictions and quarantine on the level of entire provinces (including suspension of public transportation, closures of airports, railway stations, and highways within cities), cancellation of mass gathering activities, and other measures aimed to reduce transmission of the infection [2, 3, 4].

Despite the unprecedented and robust prevention and control measures, the spread of COVID-19 was not contained to China, and the disease spread to other countries. The epidemic has been recognised by the World Health Organization (WHO) as a public health emergency of international concern on 31 January 2020, and on 11 March 2020 the WHO declared the outbreak a pandemic [5]. As of 21 March 2020, when significant intervention measures were introduced in Australia, over 285,000 cases have been confirmed worldwide, causing more than 11,500 deaths; and in a month, by 23 April, the total number has grown to exceed 2.628 million cases, with more than 183,400 deaths [6, 7]. By 21 March 2020, the disease established a sustained local transmission in many countries around the globe, with more than 180 countries and territories affected, including Italy, Spain, Iran, the United States, Germany, France, and South Korea as the top eight affected nations [6, 7]. The cumulative incidence, incidence, and the growth rate of cumulative incidence are traced for these countries, as well as Australia, in Appendix A, see Fig. 7, 8 and 9 respectively.

The scale of the COVID-19 pandemic has grown several orders of magnitude in a matter of weeks, from hundreds to thousands to tens of thousands, with the rate of these transitions varying across countries. Of particular interest to our study is the time periods when the epidemics are sustained locally in these countries, but before the effects of adopted intervention strategies are fully felt. One immediate observation is that during this period, the growth rate of cumulative incidence in many of the traced national epidemics is averaging within the range between 0.2 and 0.3, that is, there are 20% to 30% daily increases in new cases on average. This is particularly evident for Spain, France, and Germany (Fig. 8), as well as China, Iran and Italy (Fig. 7). These average estimates provide approximate "invariants" and reduce uncertainty around key epidemiological parameters, required to calibrate disease transmission models, before investigating possible effects of various intervention policies.

While worldwide public health emergencies have been declared and mitigated in the past — e.g., the "swine flu" pandemic in 2009 [8, 9, 10, 11] — the scale of socio-economic disruptions caused by the unfolding COVID-19 pandemic is unparalleled in recent history. Effects of the COVID-19 pandemic have quickly spilled over from the healthcare sector into international trade, tourism, travel, energy and finance sectors, causing a panic in the equity markets worldwide [12]. Australia has experienced most of these effects, with the number of confirmed COVID-19 cases crossing 1,000 on 21 March 2020, and doubling in numbers in three days, with the cumulative incidence growth rate trending above 20% during two weeks preceding 24 March 2020. Intervention measures introduced in Australia prevented the pandemic continuing along these trends curbing the devastating growth seen in other COVID-19 affected nations. Nevertheless, there is an ongoing debate on the utility of specific interventions (e.g., school closures), the low compliance with social distancing measures (e.g., reduction of mass gatherings), and the optimal combination of particular health intervention options balanced against social and economic ramifications, and restrictions on civil liberties. A rigorous and unbiased evaluation of available options has been, and continues to be, urgently required, and this study provides a timely input to the pandemic response planning in Australia. We quantitatively evaluate and compare several mitigation and suppression measure, using a high-resolution individual-based computational model calibrated to key characteristics of COVID-19 pandemics. In particular, this comparative analysis identifies minimal levels of social distancing compliance required for controlling COVID-19 spread in Australia in the near future, as well as trade-offs between these levels and duration of the interventions, and between the interventions' delay and their duration. Specifically, our simulations suggest

that, without an 80–90% compliance with social distancing strategies, the epidemic could not be effectively controlled, while a three-day delay in introducing such measures lengthens their required duration by almost four weeks on average.

2. Intervention strategies

Our primary objective is an evaluation of several intervention strategies that have been currently deployed in Australia, or have been considered for a deployment. It is well known that, without efficient and timely interventions, long-distance travel typically carries a virus around the globe within weeks to months of the onset of the outbreak, often causing a worldwide public health emergency [8, 9, 10, 11]. In an attempt to prevent, slow down and eradicate the spread of COVID-19, several pandemic intervention strategies, including various approaches to containment, mitigation and suppression, have been investigated, deployed, and adjusted across the world in the last months. While these strategies inevitably vary across nations, they share fundamental approaches which are adapted by national healthcare systems, aiming at a broad adoption within societies. In the absence of a COVID-19 vaccine, as pointed out by Ferguson et al. [13], *mitigation* policies may include case isolation of patients and home quarantine of their household members, social distancing of the individuals within specific age groups (e.g., the elderly, defined as older than 75 years), as well as people with compromised immune systems or other vulnerable groups. In addition, *suppression* policies may require an extension of case isolation and home quarantine with social distancing of the entire population. Often, such social distancing is supplemented by school and university closures.

Some of these intervention strategies and their combinations have shown early promise, while some have been less effective, being hindered by logistical constraints and low compliance, due to diverse factors often unique to the affected countries. For example, the model developed by the Imperial College COVID-19 Response Team have demonstrated that a combination of mitigation and suppression strategies deployed over three to five months may "reduce peak healthcare demand by 2/3 and deaths by half" [13].

In Australia, an accurate investigation and evaluation of the COVID-19 spread and possible interventions, needs to carefully include demographic specifics, since the population is concentrated mainly along the coast (around urban areas). For instance, previous modelling has suggested that an epidemic of a respiratory disease, such as influenza, typically develops in two waves, initially affecting the more densely populated urban areas, and then spreading to regional and rural areas [14, 15, 16]. In particular, as argued by Cauchemez et al. [17], "back-and-forth waves of transmission between the school, the community, and the household" demand an explicit account of distribution and structuring of schools, grades, and classes in epidemiological models of respiratory diseases.

We considered several intervention strategies: restriction on international arrivals ("travel ban"); case isolation; home quarantine of family members of the traced and isolated cases; social distancing for various population compliance levels up to and including 100% (full lockdown); and school closures. We explored these intervention strategies independently and in various combinations. Each of these scenarios was traced over time and compared to the baseline model, in an attempt to quantify their potential for the curtailing the epidemic in Australia, identify minimal levels of social distancing compliance, and determine the potential impact of school closures on the impact of intervention measures.

Restriction on international arrivals is set to be enforced from the moment when the number of confirmed infections exceeds the threshold of 2,000 cases. This concurs well with the actual epidemic timeline in Australia, which imposed a ban on all arrivals of non-residents, non-Australian citizens, from 9pm of 20 March 2020, with a requirement for strict self-isolation of returning citizens. The number of COVID-19 cases crossed 1,000 cases on 21 March 2020, and doubled to slightly over 2,000 on 24 March 2020, so the 2,000 threshold chosen on our model reflects a delay in implementing the measures, a delay in registering symptomatic cases, as well as a more nuanced distribution of imported cases which involved Australians returning home via both the air and maritime routes. The restriction on international arrivals is included in modelling of all other strategies, and is not traced independently, as this mitigation approach is not under debate.

The case isolation mitigation strategy was modelled along the lines considered in the study of the Imperial College COVID-19 Response Team [13]: 70% of symptomatic cases stay at home, reduce their non-household

contacts by 75% (so that their transmission rates decrease to 25% of the standard rate), and maintain their household contacts (i.e., their transmission rates within household remain unchanged). The home quarantine strategy for household contacts of index cases has also been considered. Unlike the home-quarantine model of Ferguson *et al.* [13], we allow compliance to vary within affected households (i.e., at the individual level). The scope of home quarantine includes 50% of individuals, limiting their non-household contacts to 25% of the standard rate, while doubling their in-household contacts. Both case isolation and home quarantine are assumed to be in force from the first day of the epidemic, as has been the case in Australia.

Social distancing (SD) has been implemented in our model by removing all working group contacts, and setting all non-household contacts to 50% of the standard rate, while keeping the contacts within households unaltered. As mentioned above, the SD compliance levels vary from the zero-SD mode to the full lockdown mode, with a fraction of agents (the SD compliance level) following these constraints. Similar to the restriction on international arrivals, the SD strategy is triggered by crossing the threshold of 2,000 cases (matching the actual timeline on 24 March 2020). An alternative threshold of 1,000 cases, matching the actual numbers reported on 21 March 2020, is considered to evaluate a delayed introduction of strong social distancing measures (Appendix G).

Finally, school closures (SC) are considered to remove both students and their teachers from school interactions (their corresponding transmission rates are set to zero), but increase their interactions within households. Such adjustments are modelled with a 50% increase of the household contacts, applied also to a randomly selected parent who chooses to stay at home, with a varying degree of commitment. Specifically, we compared 25% or 50% commitment, as in Australia there is no legal age for leaving school-age children home alone for a reasonable time, in relevant circumstances. School closures are assumed to be followed with 100% compliance, and may be concurrent with all other strategies described above. For example, they may account for scenarios when, under a partial SD compliance, some household members may choose to leave their households during daytime and interact at work, while their children and/or teacher partners (i.e., other adults) stay at home. The SC strategy is also evaluated as triggered by crossing the threshold of 2,000 cases — this is not a current practice in Australia. We note that the Australian Federal Government has not been recommending schools closures, and so we investigate the SC intervention separately from, or coupled with, the SD strategy. Hence, the evaluation of school closures provides an input to policy setting, rather than forecast changes to possible epidemic dynamics at this stage.

While the case isolation and home quarantine strategies are assumed to last during the full course of the epidemic, the duration of SD and/or SC strategies varies, across a range of time periods, with a specific focus on 49 and 91 days, that is, 7 or 13 weeks.

3. Results

We present results of the high-resolution (individual-based) pandemic modelling in Australia, using a modified and extended agent-based model, AceMod, previously developed and validated for simulations of pandemic influenza in Australia [18, 14, 15, 16]. The epidemiological component was developed and calibrated specifically to COVID-19, and then validated using the actual timeline in Australia (see Methods 6). Stochastic agent-based models (ABM) have been established as robust tools for tracing fine-grained effects of heterogeneous intervention policies in diverse epidemic and pandemic settings [19, 20, 9, 21, 8, 22, 23, 24, 25, 26], including for policy advice currently in place in the USA and the UK [13]. Importantly, a sensitivity analysis with respect to multiple parameters, e.g., describing natural history of the disease, is intrinsic to an ABM, due to heterogeneity of the agents stochastically interacting during discrete-time simulation. Robustness of our model is established by validation against actual epidemic curves, confirming that the adopted parametrization is acceptable.

The comparative analysis is carried out by AceMod, across all intervention strategies, for the calibrated set of parameters (see Methods 6), including $R_0 = 2.27$ (i.e., scaling with $\kappa = 2.75$), and the transmission and contact rates as detailed in Appendix D. The infectivity of infected agents is set to exponentially rise and peak at 5 days, after an incubation period which includes two days of zero infectivity (latent period). The symptoms are set to last up to 12 days post the infectivity peak, during which time infectiousness linearly decreases to zero — this results in the generation period around 6.4 days. The probability of

4

transmission for asymptomatic/presymptomatic agents is set as 0.3 of that of symptomatic individuals; and the age-dependent fractions of symptomatic cases are set as $\sigma_c = 0.134$ for children, and $\sigma_a = 0.669$ for adults.

3.1. Baseline

A trace of the baseline model — no interventions whatsoever — is shown in Fig. 1, with clear epidemic peaks in both incidence and prevalence evident after 105–110 days from the onset of the disease in Australia, i.e., occurring around mid-May 2020 in the absence of any interventions. The scale of the impact is very high, with nearly 50% of the Australian population showing symptoms. This baseline scenario is provided only for comparison, in order to evaluate the impact of interventions, most of which are already in place in Australia. To re-iterate, we consider timely intervention scenarios applicable to the situation in Australia at the end of March 2020, in which the number of confirmed COVID-19 cases crossed 2,000 on 24 March 2020, and the growth rate of cumulative incidence $\dot{C}$ stayed above 20% for nearly two weeks prior to that. We observe that the simulated baseline generates the 20% cumulative incidence increase, in a strong agreement with actual dynamics.

3.2. Case isolation: CI, and home quarantine: HQ

All the following interventions include restrictions on international arrivals, triggered by the threshold of 2,000 cases. Three mitigation strategies are of immediate interest: (i) case isolation, (ii) in-home quarantine of household contacts of confirmed cases, and (iii) school closures, combined with (i) and (ii). These strategies are shown in Fig. 1, with the duration of the SC strategy set as 49 days (7 weeks), starting when the threshold of 2,000 cases is reached. The case isolation coupled with home quarantine delays the epidemic peak by about 26 days on average (e.g., shifting the incidence peak from day 97.5 to day 123.2, and the prevalence peak from day 105 to day 130.7, on average), while reducing the severity at the peak time by around 47–49%. The main contributing factor is case isolation, as adding home quarantine, with 50% in-home compliance, to case isolation of 70% symptomatic individuals, delays the epidemic peak by less than three days on average. The overall attack rate resulting from the coupled policy is also reduced in comparison to the baseline scenario. However, case isolation and home quarantine alone are not effective for epidemic suppression, with prevalence still peaking in millions of symptomatic cases (1.873M), which would have completely overburdened the Australian healthcare system [27].

3.3. School closures: SC

Adding school closures to the case isolation and home quarantine approach also does not achieve a significant reduction in the overall attack rate (Fig. 1). The peaks of both incidence and prevalence are delayed by about four weeks (about 27 days for both incidence and prevalence). However, their magnitudes remain practically the same, due to a slower growth rate of cumulative incidence (Fig. 1). This is observed irrespective of the commitment of parents to stay home (Appendix F). We also traced the dynamics resulting from the SC strategy for two specific age groups: children and individuals over 65 years old, shown in Appendix F. The four-week delays in occurrence of the peaks are observed across both age groups, suggesting that there is a strong concurrence in the disease spread across these age groups. We also observe that under the SC strategy coupled with case isolation and home quarantine, the magnitude of the incidence peak for children increases by about 7% shown in Appendix F, Fig. 12. This may be explained by increased interactions of children during various household and community social mixing, when schools are closed. Under this strategy, there is no difference in the magnitude of the incidence peak for the older age group (Appendix F, Fig. 13). We also note that the considered interventions succeed in reducing a relatively high variance in the incidence fraction of symptomatic older adults, thus, reducing the epidemic potential to adversely affect this age group specifically.

In short, the only tangible benefit of school closures, coupled with case isolation and home quarantine, is in delaying the epidemic peak by four weeks, at the expense of a slight increase in the contribution of children to the incidence peak. Given other societal costs of school closures (e.g., drawing their parents employed in healthcare and other critical infrastructure away from work), this strategy may be less effective
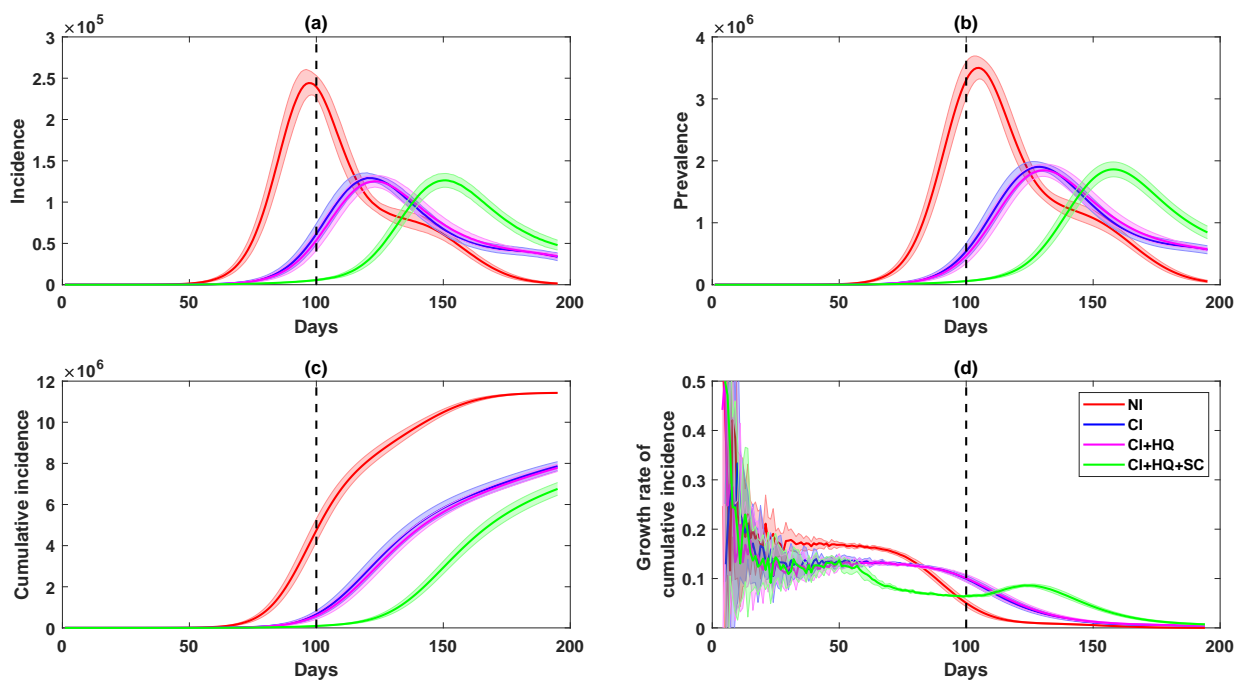
Figure 1: A combination of the case isolation and home quarantine measures delays epidemic peaks and reduce their magnitude, whereas school closures have short-term effect. Several baseline and intervention scenarios, traced for incidence (a), prevalence (b), cumulative incidence (c), and the growth rate of cumulative incidence $\dot{C}$ (d), shown as average (solid) and standard deviation (shaded) profiles, over 10 runs. The strategy with school closures (SC) combined with case isolation lasts 49 days (7 weeks), marked by a vertical dashed line. Restrictions on international arrivals are set to last until the end of each scenario.
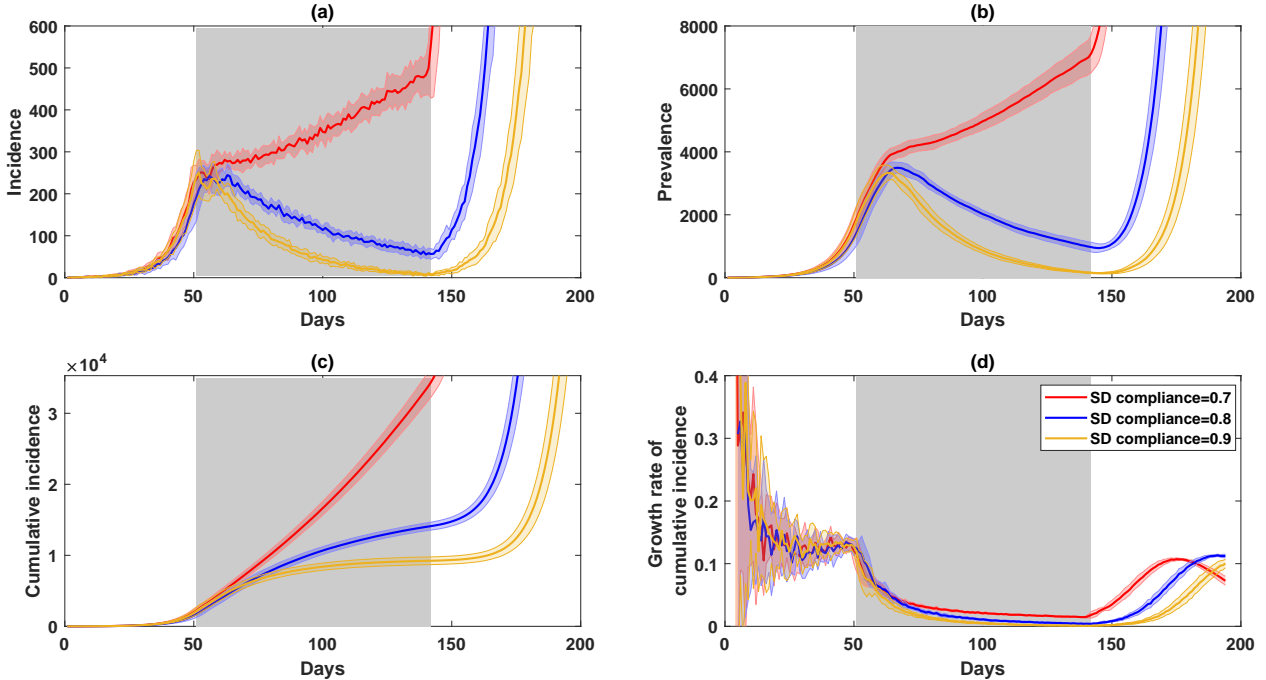
Figure 2: Strong compliance with social distancing (at 80% and above) effectively controls the disease during the suppression period, while lower levels of compliance (at 70% or less) do not succeed for any duration of the suppression. A comparison of social distancing strategies, coupled with case isolation, across different compliance levels (70%, 80% and 90%). Duration of each social distancing (SD) strategy is set to 91 days (13 weeks), shown as a grey shaded area. Case isolation, home quarantine and restrictions on international arrivals are set to last until the end of each scenario. Traces include incidence (a), prevalence (b), cumulative incidence (c), and the growth rate of cumulative incidence $\dot{C}$ (d), shown as average (solid) and standard deviation (shaded) profiles, over 10 runs.

than previously suggested (e.g., school closures are considered an important part of pandemic influenza response). There is, nevertheless, one more possible benefit of school closures, discussed in the context of the overall social distancing, as described below.

3.4. Social distancing: SD

Our next step is to compare social distancing strategies, coupled with case isolation, across different compliance levels. Low compliance levels, set at less than 70%, did not show any potential to suppress the disease in the considered time horizon (28 weeks), while the total lockdown, that is, complete social distancing at 100%, managed to reduce the incidence and prevalence to zero, after 49 days of the mitigation. However, since the total lockdown is never perfect, we focus on the practically achievable compliance levels: 70%, 80% and 90%, with their duration set to 91 days (13 weeks), shown in Fig. 2 .

Importantly, during the time period that the SD level is maintained at 70%, the disease is not controlled, with the numbers of new infected cases (incidence) remaining in hundreds, and the number of active cases (prevalence) remaining in thousands. Thus, 70% compliance is inadequate for reducing the effective reproductive number below 1.0. In contrast, the two higher levels of SD, 80% and 90%, are more effective at suppressing both prevalence and incidence during the 13-week social distancing period.

Figure 2 contrasts these three levels of SD compliance, "zooming in" into the key time period, immediately following the introduction of social distancing. Crucially, there is a qualitative difference between the lower

levels of SD compliance (70%, or less), and the higher levels (80%, or more). For the SD compliance set at 80% and 90%, we observe a *reduction* in both incidence and prevalence, lasting for the duration of the strategy (91 days). The 80% SD compliance does not completely eliminate the disease, but reduces the new cases to less than 100, with prevalence below 1,000 (during the suppression period, before a possible resurgence). This level of compliance would succeed in eliminating the disease in Australia if the strategy was implemented for a longer period, e.g., another 4–6 weeks.

The 90% SD compliance practically controls the disease, bringing both incidence and prevalence to very low numbers of isolated cases (and reducing the effective reproductive number to nearly zero). It is possible for the epidemic to spring back to significant levels even under this level of compliance, as the remaining sporadic cases indicate a potential for endemic conditions. We do not quantify these subsequent waves, as they develop beyond the immediately relevant time horizon. Nevertheless, we do share the concerns expressed by the Imperial College COVID-19 Response Team: "The more successful a strategy is at temporary suppression, the larger the later epidemic is predicted to be in the absence of vaccination, due to lesser build-up of herd immunity" [13].

The cumulative incidence for the best achievable scenario (90% SD compliance coupled with case isolation, home quarantine, and restrictions on international arrivals) settles in the range of 8,000 – 10,000 cases during the suppression period, before a possible resurgence, at some point after intervention measures are relaxed. This is an outcome several orders of magnitude better than the worst case scenario, developing in the absence of the combined mitigation and suppression strategies.

The considered scenarios in which social distancing measures are triggered by 2,000 confirmed cases, aligned with the actual epidemic curve in Australia, are also compared with an alternative scenario triggered by threshold of 1,000 cases which could have initiated the strict suppression earlier (Appendix G). The best agreement between the actual and simulation timelines is found to match a delayed but high (90%) SD compliance, appearing to be followed from 24 March 2020, after a three-day period with a weaker compliance which commenced on 21 March 2020 when the travel restrictions were introduced.

Differences between 70% and 90% SD compliance levels are also visualised, for the alternative threshold scenario, in choropleth maps of four largest Australian Capital Cities: Sydney, Melbourne, Brisbane and Perth, shown in Appendix H, at day 60, that is, at a time when these two compliance levels result in a tangible divergence.

It is clear that there is a trade-off between the level of SD compliance and the duration of the SD strategy: the higher the compliance, the more quickly incidence is suppressed. Both 80% and 90% compliance levels control the spread within reasonable time periods: 18-19 and 13-14 weeks respectively. In contrast, lower levels of compliance (at 70% or less) do not succeed for any duration of the imposed social distancing limits. This quantitative difference is of major policy setting importance, indicating a sharp transition in the performance of these strategies in the region between 70% and 80%. Referring to Fig. 3, the identified transition across the levels of compliance with social distancing may also be interpreted as a tipping point or a phase transition [28, 15, 29]. In particular, there is a similarity to percolation transition in a forest-fire model with immune trees [30, 31, 32]. A transition we detect between 70% and 80% SD compliance levels (i.e., at some percolation threshold), separates distinct epidemic phases, with the critical regime exhibiting the effective reproductive number $R_0 = 1.0$. It is precisely this regime passing which signifies moving into the phase achieving control of the epidemic, i.e., reducing R_0 below 1.0.

We do not attempt to establish a more precise level of required compliance, e.g., 75%. Such a precision would be of lesser practical relevance than the identification of 80% level as the minimal acceptable level of social distancing, with 90% providing a shorter timeframe. Notably, a three-day delay in introducing strong social distancing measures is projected to require an approximately four-week longer suppression period, beyond 91 days considered in the primary scenario (Appendix G).

At this stage we revisit school closures. As shown in Fig. 4, addition of the SC strategy to SD set at 70% also generates a reduction in incidence, albeit progressing at a higher level than such reductions observed at 80% and 90% SD levels, coupled with school closures. This suggests that another potential benefit of school closures is that it may "compensate" for about 10% lack of SD compliance. This combination, however, would require a much longer duration of the coupled strategy (70% SD and SC), and may be impractical.

Finally, we report fractions of symptomatic cases across mixing contexts (Appendix I), with the commu-
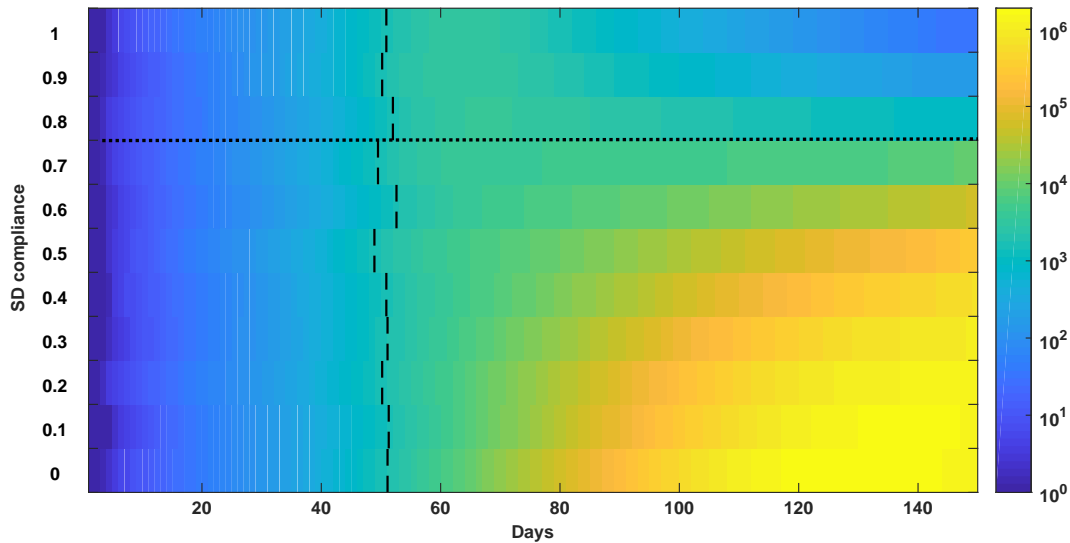
Figure 3: Colour image plot of disease prevalence as a function of time (horizontal axis) and social distancing (SD) compliance (vertical axis). A phase transition is observed between 70% and 80% SD compliance (marked by a dotted line). For SD compliance levels below 80%, the prevalence continues to grow after social distancing is implemented, while for compliance levels at or above 80% the prevalence declines, following a peak formed after approximately two months. The colours correspond to log-prevalence, traced from the epidemic's onset until the end of the suppression period. Vertical dashes mark the time when threshold of 2,000 is crossed, triggering SD, averaged over 10 runs for each SD level.

nity transmission through households being predominant for the considered scenarios, and steadily increasing with the strengthening of SD compliance, from 30.4% (the household fraction under case isolation and home quarantine) to 47.6% (full lockdown).

3.5. Summary

In short, the best intervention approach identified by AceMod is to combine restrictions on international arrivals (already implemented in Australia), case isolation and home quarantine (also already implemented to a reasonable extent, but demanding increasing testing and monitoring resources in order to achieve an elimination of the community transmission), and social distancing with at least 80%–90% compliance and a duration of 91 days (13 weeks). A lower compliance level is found to result in a higher prevalence at the end of suppression period, which would require an extension of intervention measures in order to achieve the elimination.

We point out that our results are relevant only for the duration of the mitigation and suppression, and a resurgence of the disease is possible once these interventions cease, as shown in Fig. 2. We also note that a rebound in the incidence and prevalence post-suppression period is not unavoidable: more efficient and large-scale testing methods are expected to be developed in several months, and so the resultant contact tracing and case isolation are likely to prevent a resurgence of the disease. The international travel restrictions are assumed to stay in place. Hence, we do not quantify the precise impact of control measures beyond the selected time horizon (28 weeks), and focus on the time period in the near future, aiming to provide immediately relevant insights. Furthermore, our results should not be seen as policies optimised over all possible parameter combinations, but rather as a clear demonstration of the extent of social distancing required to reduce incidence and prevalence in the next two to six months.
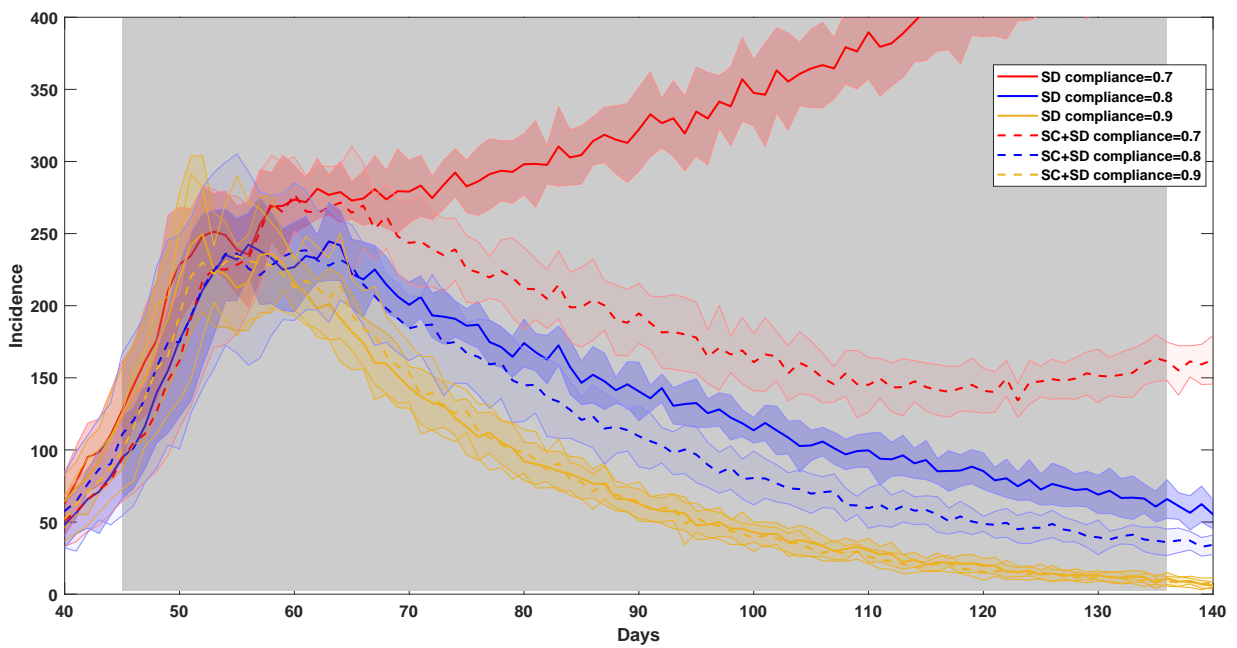
Figure 4: School closures may "compensate" for about 10% lack of social distancing (SD) compliance. A comparison of social distancing strategies, coupled with case isolation, home quarantine, and school closures (SC) or no school closures, across different compliance levels (70%, 80% and 90%), shown as average (solid) and standard deviation (shaded) profiles, over 10 runs. Duration of each combined SD and SC strategy is set to 91 days (13 weeks), shown as a grey shaded area. Case isolation, home quarantine and restrictions on international arrivals are set to last until the end of each scenario.

4. Conclusions

In this study we simulated several possible scenarios of COVID-19 pandemic's spread in Australia. The model, AceMod, was calibrated to known pandemic dynamics, and accounted for age-dependent attack rates, a range of reproductive numbers, age-stratified and social context dependent transmission rates, household clusters and other social mixing contexts, symptomatic-asymptomatic distinction, long and varying incubation periods, and other relevant epidemiological parameters.

An important calibration result was the need for age-dependent fractions of symptomatic agents, with the fraction of symptomatic children found to be one-fifth of that of the adults. While other combinations of parameters may also succeed in calibration, setting the *age-dependent* fractions of symptomatic cases may be important for other modelling studies across the world.

An analysis of spatiotemporal characteristics of COVID-19 pandemic in Australia was carried across a range of intervention strategies, some of which are already in place, while some are under discussion. By running multiple computer simulations, while varying details of the micro-simulation, we estimate epidemic dynamics, in terms of the infection's prevalence and incidence, its peaks and waves, and other indicators, including age-dependent attack rates.

We reported several findings relevant to COVID-19 mitigation and suppression policy setting. The first implication is that the effectiveness of school closures is limited, producing a four-week delay in epidemic peak, without a significant impact on the magnitude of the peak, in terms of incidence or prevalence. The temporal benefit of this delay may be offset not only by logistical complications, but also by some increases in the fractions of both children and older adults during the period around the incidence peak.

The second implication is related to the social distancing (SD) strategy, which showed little benefit for lower levels of compliance (at 70% or less) — these levels do not contribute to epidemic control for any duration of the social distancing restrictions. Only when the SD compliance levels exceed 80%, there is a reduction in incidence and prevalence. Our modelling results indicate existence of an actionable transition across these strategies in the range between 70% and 80%. In other words, increasing a compliance level just by 10%, from 70% to 80%, may effectively control the spread of COVID-19 in Australia, by reducing the effective reproductive number to near zero (during the suppression period). We also reported a trade-off between the compliance levels and the duration of SD mitigation, with 90% compliance significantly reducing incidence and prevalence after a shorter period of 91 days (13 weeks). Although a resurgence of the disease is possible once these interventions cease, we believe that this study could facilitate a timely planning of effective intervention strategies.

Future research will address several limitations of our study, including a more fine-grained implementation of natural history of the disease, incorporation of more recent ABS data from 2020, and an account of in-hospital transmissions. We also hope to trace specific spatial pathways and patterns of epidemics, in order to enable a detailed understanding of how the infection spreads in diverse circumstances and localities, with the aim to identify the best ways to locate and curtail the pandemic spread in Australia. Other avenues lead to analysis of precursors and critical thresholds for possible emergence of new strains, as well as various "change points" in the spreading rate [33, 34, 28, 35], studies of genomic surveillance data interpreted as complex networks [36, 37, 38, 39, 40], dynamic models of social behaviour in times of health crises [41, 15, 42, 43, 44, 45], and investigations of global socioeconomic effects of the COVID-19 pandemic [46, 47].

5. Acknowledgments

6. Methods

AceMod, the *Australian Census-based Epidemic Model*, employs a discrete-time and stochastic agent-based model to investigate complex outbreak scenarios across the nation over time. The AceMod simulator comprises over 24 million software agents, each with attributes of an anonymous individual (e.g., age, gender, occupation, susceptibility and immunity to diseases), as well as contact rates within different social contexts (households, household clusters, local neighbourhoods, schools, classrooms, workplaces). The set of generated agents captures average characteristics of the real population, e.g., AceMod is calibrated to the Australian Census data (2016) with respect to key demographic statistics. In addition, the AceMod simulator has integrated layered school attendance data from the Australian Curriculum, Assessment and Reporting Authority (ACARA), within a realistic and dynamic interaction model, comprising both mobility and human contacts. These social mixing layers represent the demographics of Australia as close as possible to the Australian Bureau of Statistics (ABS) and other datasets, as described in Appendix E.

Potential interactions between spatially distributed agents are represented using data on mobility in terms of commuting patterns (work, study and other activities), adjusted to increase precision and fidelity of commute networks [48]. Each simulation scenario runs in 12-hour cycles ("day" and "night") over the 196 days (28 weeks) of an epidemic, and agents interact across distinct social mixing groups depending on the cycle, for example, in working groups and/or classrooms during a "day" cycle, and their households, household clusters, and local communities during the "night" cycle. The interactions result in transmission of the disease from infectious to susceptible individuals: given the contact and transmission rates, the simulation computes and updates agents' states over time, starting from initial infections, seeded in international airports around Australia [18, 14]. The simulation is implemented in C++11, running on a High Performance Computing (HPC) service and utilising 4264 cores of computing capacity.

Simulating disease transmission in AceMod requires both (i) specifics of local transmission dynamics, dependent on individual health characteristics of the agents, such as susceptibility and immunity to disease, driven by their transmission and contact rates across different social contexts; and (ii) a natural disease history model for COVID-19, i.e., the infectivity profile from the onset of infection, over an incubation period, to the peak of infectivity, to recovery, for a single symptomatic or asymptomatic individual. It is precisely this part of the model which demands a careful study and calibration to available estimates of key transmission characteristics of COVID-19 spread.

Despite several similarities with influenza, COVID-19 has a number of notable differences, specifically in relation to transmissions across children, its reproductive number R_0, incubation and generation periods, proportion of symptomatic to asymptomatic cases [49, 50], the infectivity of the asymptomatic and presymptomatic individuals, etc. (see Appendix B). While uncertainty around the reproductive number R_0, the incubation and generation periods, as well as the age-dependent attack rates of the disease, have been somewhat reduced [3, 4, 51], there is still an ongoing effort in estimating the extent to which people without symptoms, or exhibiting only mild symptoms, might contribute to the spread of the coronavirus [52]. Furthermore, the question whether the ratio of symptomatic to total cases is constant across age groups, especially children, has not been explored in studies to date, remaining another critical unknown.

Thus, our first technical objective was to calibrate the AceMod model for specifics of COVID-19 pandemic, in order to determine key disease transmission parameters of AceMod, so that the resultant dynamics concur with known estimates. In particular, we aimed to stay within a range of the reproductive number (the number of secondary cases arising from a typical primary case early in the epidemic) $R_0 = [2.0, 2.5]$, which has been reported by the WHO-China Joint Mission on Coronavirus Disease 2019 [3]. Several recent studies estimated that before travel restrictions were introduced in Wuhan on 23 January 2020, the median daily reproduction number R_0 in Wuhan was 2.35, with 95% confidence interval of $(1.15 - 4.77)$ [53]. An agent-based model of the Imperial College COVID-19 Response Team used a baseline assumption that $R_0 = 2.4$, while examining values between 2.0 and 2.6 [13].

12

In our model, R_0 was investigated in the range between 1.6 and 2.8, by varying a scaling factor κ responsible for setting the contagiousness of the simulated epidemic, as explained in Appendix C [18, 15]. The value of $R_0 = 2.27$ ($\kappa = 2.75$) was found to produce the closest match to our target calibration variables, as shown in Figure 5.

We maintained the incubation period (the interval from the infection to the onset of disease in an individual) around the mean value of 5.0 days, as reported in several studies, e.g., the mean incubation period was reported as 5.2 days, 95% confidence interval (CI), 4.1 to 7.0 [54], while being distributed around a mean of approximately 5 days within the range of 2–14 days with 95% CI [55].

Importantly, we aimed to keep the resultant growth rate of cumulative incidence $\dot{C}$ around 0.2, in order to be consistent with the disease dynamics reported internationally. Another key constraint was a low attack rate in children, reported to be in single digits. For example, only 2.4% of all reported cases in China were children, while a study in Japan observed that "it is remarkable that there are very few child cases aged from 0–19 years", with only 3.4% of all cases in this age group [56]. In doing the calibration, we varied several "free" variables, such as transmission and contact rates, the fraction of symptomatic cases (making it *age-dependent*), the probability of transmission for both symptomatic and asymptomatic agents, and the infectivity profile from the onset of infection.

In calibrating these variables, we minimised changes in order to represent acceptable epidemiological characteristics. For example, we aimed for the generation period (the interval, in days, between successive onsets of symptoms along a transmission chain) to stay in the range $[6.0, 10.0]$ [54, 57, 13]. This is in line with the reported mean serial interval of 7.5 days (with 95% CI of 5.3 to 19) [54] and the 6.5-day mean generation time reported by the Imperial College COVID-19 Response Team [13]. We set the symptoms' duration after the peak of infectivity around the mean value of 12.0 days, on a linearly decreasing profile from the peak. The best match in our calibration, corresponding to $R_0 = 2.27$, was found to produce the generation period of 6.4 days.

The contact and transmission rates across various mixing contexts have been mostly set as in pandemic influenza [18], with the following notable exceptions, as detailed in Appendices C and D. The probability of transmission for asymptomatic/presymptomatic agents was set as 0.3 of that of symptomatic individuals (lower than in the AceMod influenza model). Both symptomatic and asymptomatic profiles were changed to increase exponentially after a latent period of two days, to the infectivity peak, set at the end of the incubation period, see Appendix C.

The fraction of symptomatic cases was set to two-thirds of the total cases ($\sigma = 0.669$), which concurs with several studies. For example, the initial data on 565 Japanese citizens evacuated from Wuhan, China, who were symptom-screened and tested, indicated that 41.6% were asymptomatic, with a lower bound estimated as 33.3% (95% CI: 8.3%, 58.3%) [58]. The proportion of asymptomatic cases on the Diamond Princess cruise ship was estimated in the range between 17.9% (95% credible interval (CrI):15.5–20.2%) to 39.9% (95% CrI: 35.7–44.1%) [59], noting that most of the passengers were 60 years and older, and more likely to experience more symptoms. The modelling study of Ferguson et al. [13] also set the fraction of symptomatic cases to $\sigma = 0.669$.

However, we found that the best calibration is achieved when this fraction is *age-dependent*, with the fraction of symptomatic cases among children calibrated to one-fifth of the one for adults, that is, $\sigma_c = 0.134$ for children, and $\sigma_a = 0.669$ for adults. This calibration outcome *per se* is in agreement with the reported low attack rates in children worldwide, and the observation that "children are at similar risk of infection as the general population, though less likely to have severe symptoms" [60]. Another study of epidemiological characteristics of 2,143 pediatric patients in China noted that over 90% of patients were asymptomatic, mild, or moderate cases [61]. In our study, the attack rates in children have converged to 6%, as shown in Figure 6, that is, only 6% of infections are detected in children, even with a relatively high reproductive number $R_0 > 2.0$ and a relatively long generation period of 6.4 days (in comparison, the generation period for influenza varies in AceMod in the range from 3.35 to 3.39 days).

In summary, this combination of parameters resulted in the dynamics that matched several COVID-19 pandemic characteristics, producing the rate $\dot{C}$ of cumulative incidence during a period of sustained local transmission (i.e., days 40 to 80 since the onset) in the range $[0.15, 0.2]$, as shown in Figure 5. This was achieved while keeping the attack rate in children just over 5%, and agreeing with established range of R_0,
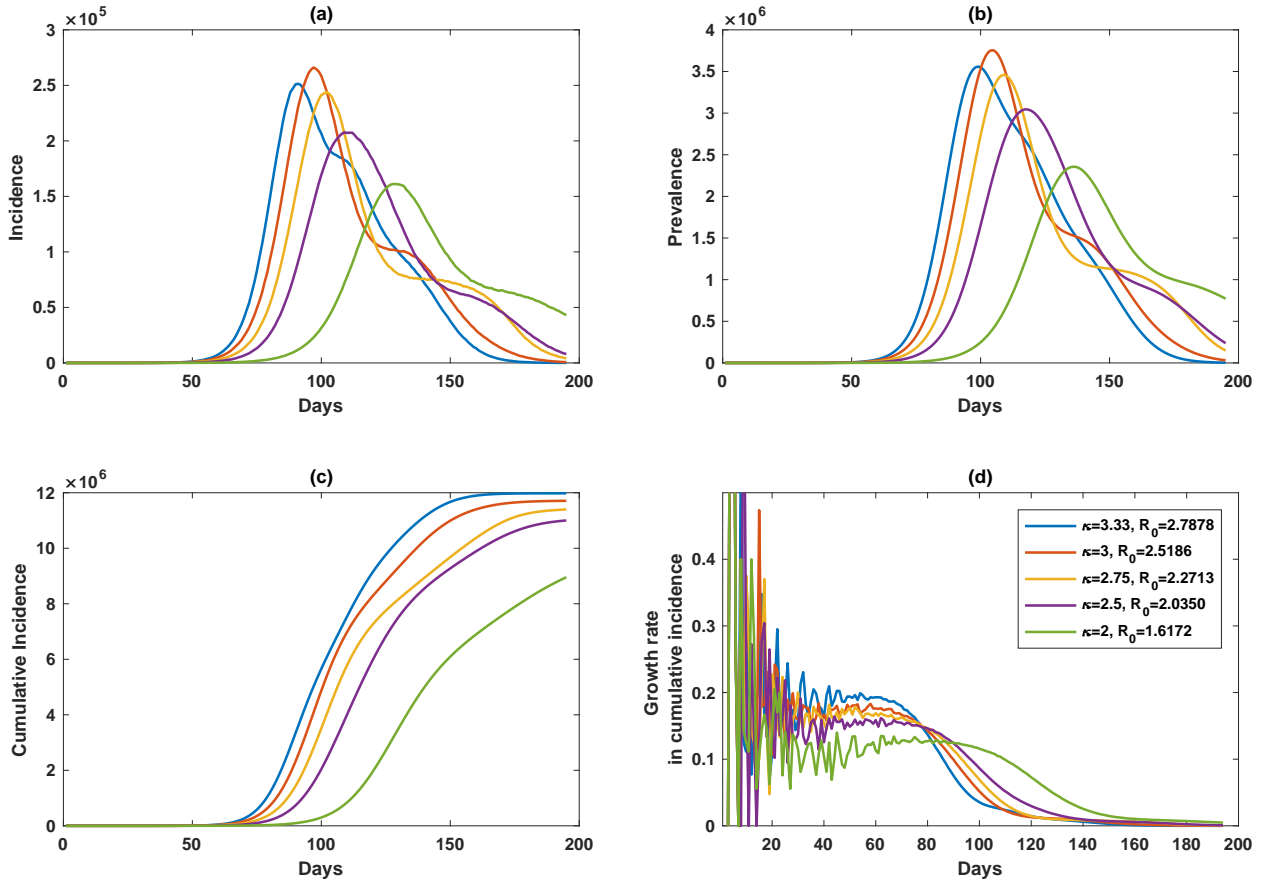
Figure 5: Calibration of AceMod parameters to the expected growth rate of cumulative incidence $\dot{C}$ (d), while varying scaling factor κ (proportional to the reproductive number R_0), with incidence (a), prevalence (b), and cumulative incidence (c).

and the incubation and generation periods.

A. COVID-19 pandemic in top 8 affected countries and Australia

Figures 7 and 8 trace cumulative incidence C, incidence, and growth rate of cumulative incidence $\dot{C} = [C(n+1) - C(n)]/C(n)$, for time step n, for the top eight affected countries (as of 21 March 2020): China, Iran, Italy, South Korea (Fig. 7), Spain, Germany, France, USA (Fig. 8). The time series begin from the day when the total number of confirmed cases exceeds five. Figure 9 traces these time series for Australia. We point out that the fraction of imported cases in the overall transmission has been fairly high in Australia, dominating the community transmission, and so we paid particular attention to the growth rate in countries where the disease was also introduced predominantly through the air travel (i.e., down-weighting the rates in China and South Korea).

B. Natural history of disease

The natural history of disease is a description of the disease from pathological onset to recovery from the perspective of a single individual, profiling their infectiousness over time. In the past, the AceMod
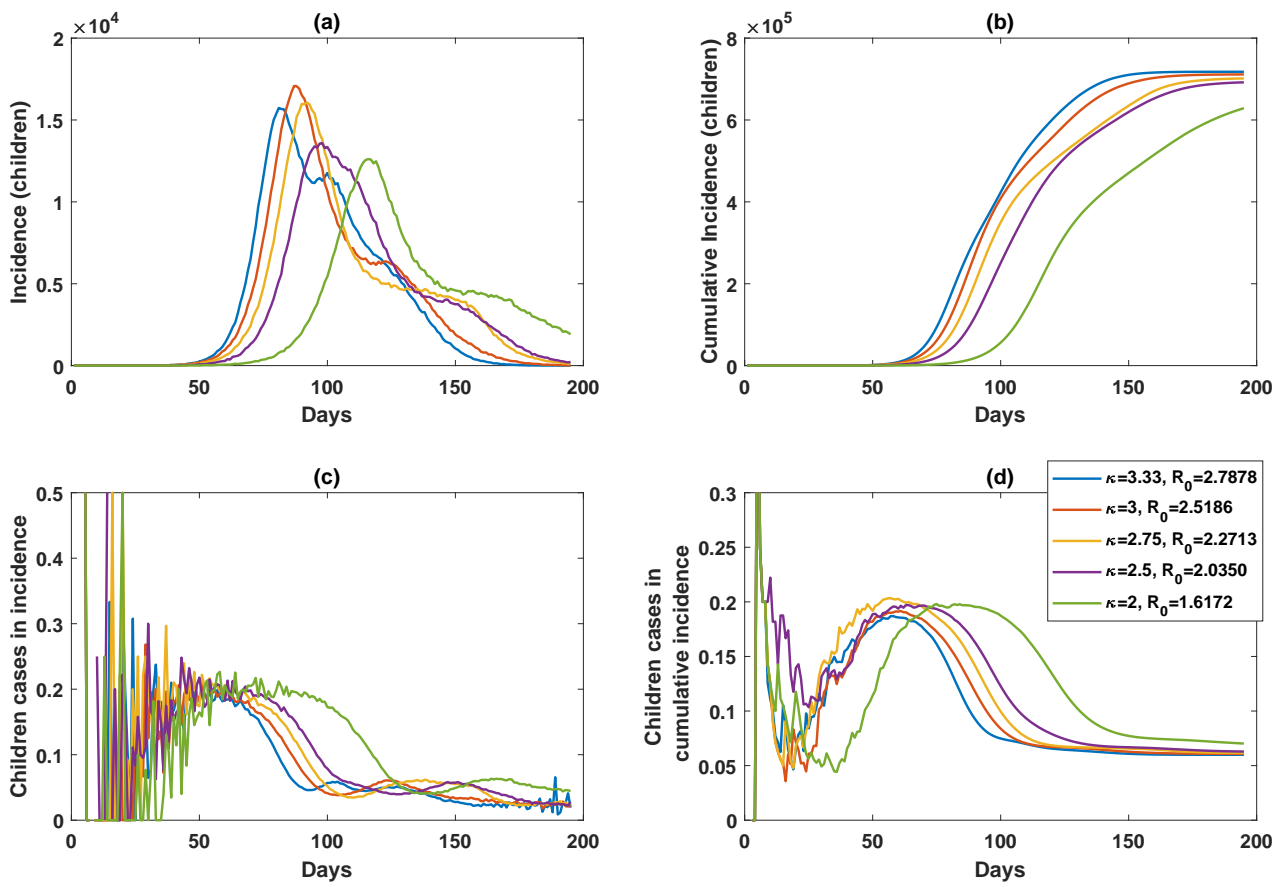
14

Figure 6: Calibration of AᴄᴇMod parameters to the attack rate in children (d), while varying scaling factor κ (i.e, reproductive number R_0), with incidence (a), prevalence (b), and cumulative incidence (c) in children.
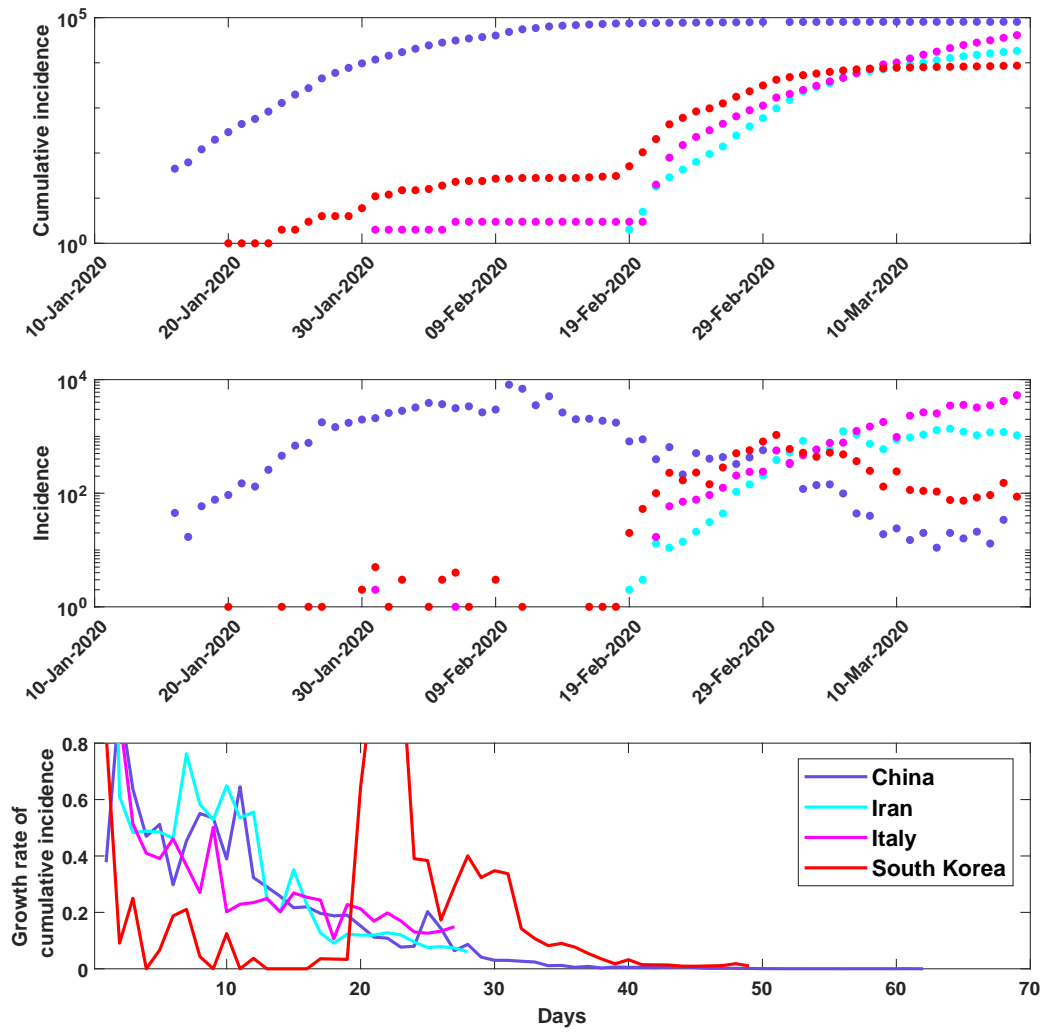
Figure 7: Cumulative incidence (log scale), incidence (log scale), and growth rate of cumulative incidence: China, Iran, Italy, South Korea (up to 19 March 2020). Days: since the day when the total number of confirmed cases exceeded five. Data sources: [62, 63].
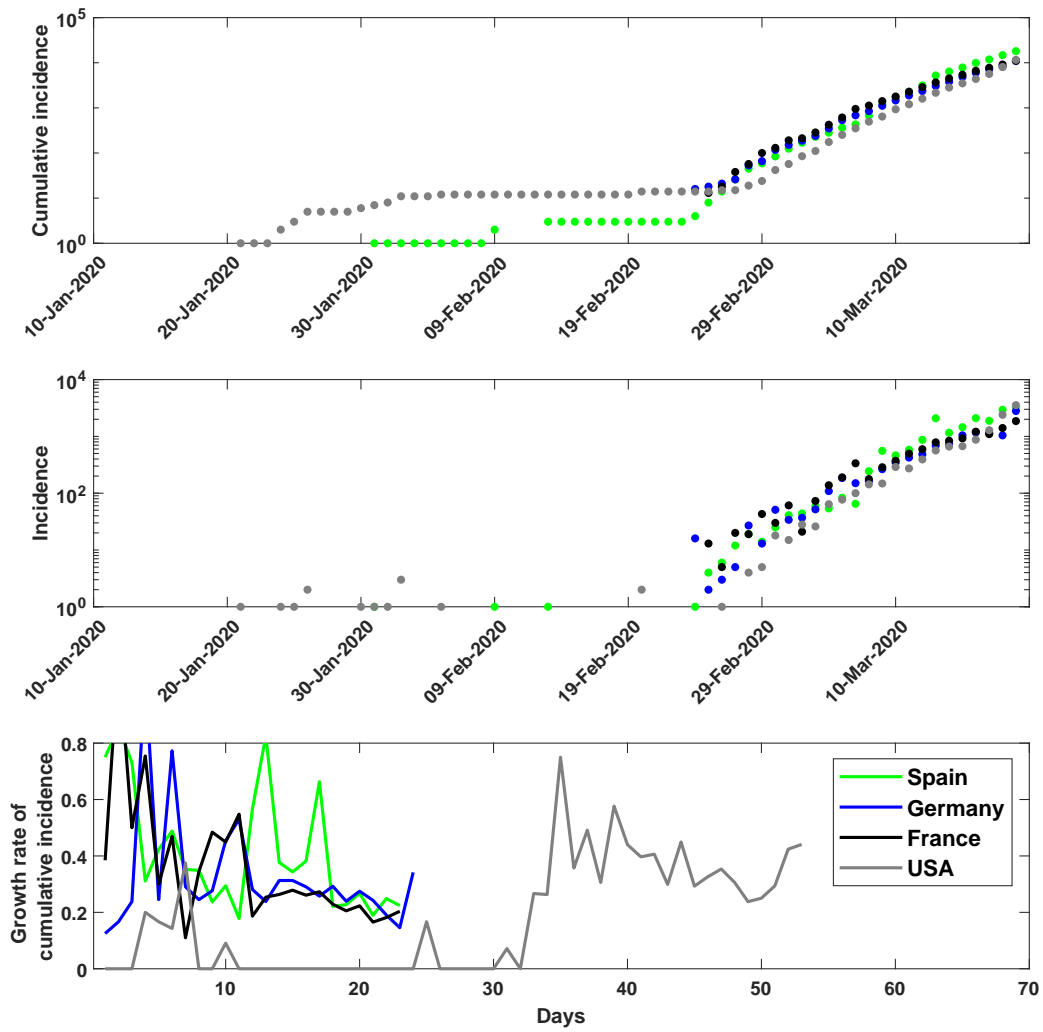
Figure 8: Cumulative incidence (log scale), incidence (log scale), and growth rate of cumulative incidence: Spain, Germany, France, USA (up to 19 March 2020). Days: since the day when the total number of confirmed cases exceeded five. Data sources: [63].
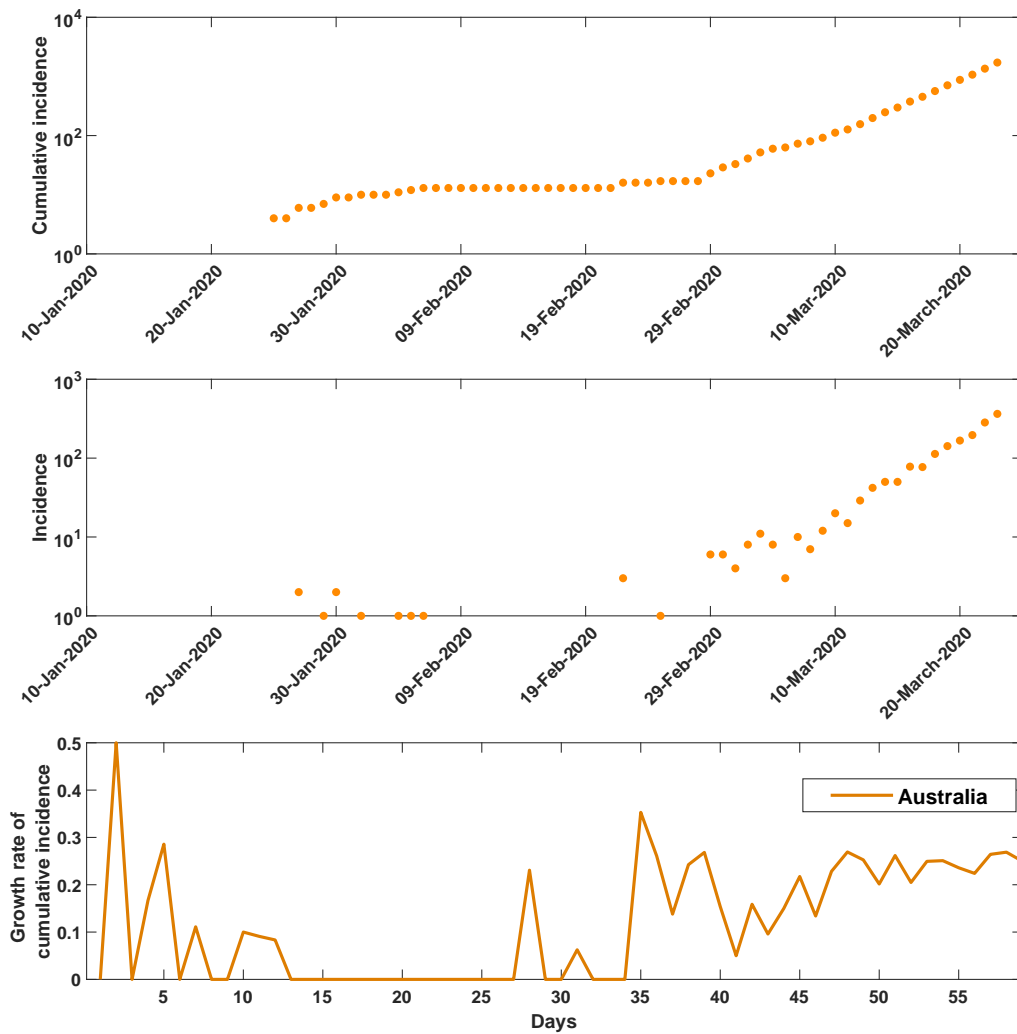
17

Figure 9: Cumulative incidence (log scale), incidence (log scale), and growth rate of cumulative incidence: Australia (up to 24 March 2020). Days: since the day when the total number of confirmed cases exceeded five. Data sources: [64].

simulator has been used to model pandemic influenza within Australia, and here we detail modifications of the natural history aimed to account for COVID-19 specifics. The natural history model considers three distinct phases of infection. The first phase is the LATENT period during which individuals are infected but unable to infect others, set in the COVID-19 model as two days. The second phase is the INCUBATION period, characterised by the onset of symptoms and an increasing infectivity, set in the COVID-19 model to lasts for five days. We model this increase in infectiousness as an exponential increase which varies from 0% to 100% over three days (see Fig. 10). Following the incubation phase, the infectious reaches its peak, and then decreases linearly over 12 more days, until the recovery, with immunity, occurs after 17 days. Finally, we assume that asymptomatic cases are 30% as infectious as symptomatic cases. Unlike influenza, where we assume that the asymptomatic fraction is the same for adults as for children, for the SARS-COV-2 coronavirus we assume that while 67% of adult cases are symptomatic, a significantly lower fraction (13.4%) is symptomatic in children.
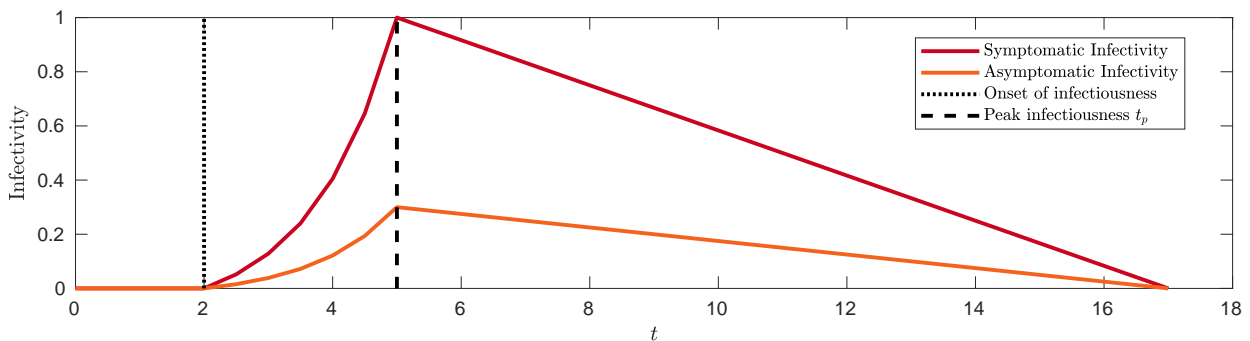

Figure 10: Profile of the infectivity used as the natural history of COVID-19, for both symptomatic and asymptomatic cases. After two days, individuals become infectious, with the infectivity rising exponentially until its peak at five days. After this peak, the infectivity linearly decreases, with full recovery occurring at 17 days. At comparable points within the natural history of disease, asymptomatic individuals are 30% as infectious as symptomatic individuals.

C. Transmission model and reproductive number

The primary dynamics of ACEMod are the infection transmissions. At each time-step the simulator determines the probability of infection for an individual, based on the infection levels in each of their mixing contexts. At each time step we consider all daytime or all nighttime contexts. Let $X_i(n)$ be a random variable describing the state of individual i at time step n. At each time step we calculate $p_i(n) = P(X_i(n) = \text{LATENT} | X - i(n-1) = \text{SUSCEPTIBLE})$, the probability that a susceptible individual is infected at n. Each individual belongs to a number of mixing groups with which an agent interacts, denoted $g \in \mathcal{G}_i(n)$, as well as an associated static set of agents $\mathcal{A}_g$. Within each of these contexts, we define a probability $p_{j \to i}^g$ that individual j infects individual i in context g in a single time step. The probability that a susceptible agent i is infected at a given time step n is thus calculated as:

$$p_i(n) = 1 - \prod_{g \in G_i(n)} \left[\prod_{j \in \mathcal{A}_g \setminus i} (1 - p_{j \to i}^g(n)) \right], \tag{1}$$

where $p_{j \to i}^g$ is the context-dependent probability that infected individual j infects susceptible agent i in mixing group g. We also define a scaling factor κ (proportional to the reproductive number R_0), as a free parameter which allows us to vary the contagiousness of simulated epidemic scenarios:

$$p_{j \to i}^g(n) = \kappa \, f(n - n_j \mid j, i) \, q_{j \to i}^g \tag{2}$$

where n_j denotes the time when agent j becomes infected, and $q_{j \to i}^g$ is the probability of transmission from agent j to i at the infectivity peak, derived from the transmission or contact rates. This model

Table 1: Daily contact probabilities $c_{j \to i}^{g}$ for different contact groups g, reported by [25], reproduced from [18], except for the rates in household clusters.

Mixing group g	Infected individual j	Susceptible individual i	Contact probability $c_{j \to i}^{g}$
Household cluster	Child (<19)	Child (<19)	0.05
	Child (<19)	Adult (>18)	0.05
	Adult (>18)	Child (<19)	0.05
	Adult (>18)	Adult	0.05
Working Group	Adult (19-64)	Adult (19-64)	0.05
Neighbourhood	Any	Child (0-4)	0.0000435
	Any	Child (5-18)	0.0001305
	Any	Adult (19-64)	0.000348
	Any	Adult (65+)	0.000696
Community	Any	Child (0-4)	0.0000109
	Any	Child (5-18)	0.0000326
	Any	Adult (19-64)	0.000087
	Any	Adult (65+)	0.000174

assumes that for all contexts, the probabilities of infection over a given time period are known. In cases where this information is unavailable, we instead utilise contact rates reported and calibrated in previous studies. Thus, a majority of the transmission and contact probabilities follow our previous work on pandemic influenza [65, 66, 25, 17, 18, 14], see Tables 1 and 2 in Appendix D. Full details regarding their application can be found in [18].

In this study we used "the attack rate pattern weighted index case" to calculate R_0 [22, 16]. The method is based on age-specific attack rates, computed as averages over many simulation instances, in order to reduce the bias in determining a typical index case, present due to population heterogeneity. As argued in [67, 16], given the correlation between age group and population structure, the age-stratified weights, assigned to secondary cases produced by a sample of index cases, improve the estimation of the reproductive number R_0.

D. Transmission and contact probabilities

Following [18], with some minor adjustments, the transmission and contact probabilities are given in Tab. 1 and Tab. 2, respectively.

E. Population generation, demographics and mobility

Prior to the AceMod simulations, a surrogate population was generated to match coarse-grained distributions arising from the 2016 Australian census, published by the Australian Bureau of Statistics (ABS). In particular we use Statistical Areas (SA1 and SA2) level statistics [68] regarding age, household composition and workplaces in generating this surrogate population. Individuals in the population are separated into 5 different age groups preschool aged children (0-4), children (5-18), young adults (19-29), adults (30-65) and older adults (65+). Along with these assigned characteristics, individuals are assigned a number of mixing contexts based on the census data. The AceMod simulator is a discrete-time simulation, where each simulated day is separated into two distinct portions: 'daytime' and 'nighttime'. In the daytime, workplace and school-based mixing are considered, whereas nighttime mixing considers household spread, and other local spread at the neighborhood (SA1) and community (SA2) levels.

The population generation begins with the contexts needed for nighttime mixing, which can be thought of as "home regions". The simulation iterates through each SA1, creating a cumulative density function (CDF) describing the size and type of households expected based on two dependent probability distributions defined by the ABS. Given this CDF, the procedure begins to randomly generate households, with the generation

Table 2: Daily transmission probabilities $q_{j \to i}^{g}$ for different contact groups g, reported by [17], reproduced from [18].

Contact Group g	Infected Individual j	Susceptible Individual i	Transmission Probability $q_{j \to i}^{g}$
Household size 2	Any	Child (<19)	0.0933
	Any	Adult (>18)	0.0393
Household size 3	Any	Child (<19)	0.0586
	Any	Adult (>18)	0.0244
Household size 4	Any	Child (<19)	0.0417
	Any	Adult (>18)	0.0173
Household size 5	Any	Child (<19)	0.0321
	Any	Adult (>18)	0.0133
Household size 6	Any	Child (<19)	0.0259
	Any	Adult (>18)	0.0107
School	Child (<19)	Child (<19)	0.000292
Grade	Child (<19)	Child (<19)	0.00158
Class	Child (<19)	Child (<19)	0.035

of agents occurring during this process. Once a household is generated for an SA1, agents are generated to match the size and type of the household (e.g., a single parent family of size four will generate one adult and three children). In order to generate attributes for this surrogate population, the simulation then reads in CDFs describing the population statistics of the given SA, with each of these agents being assigned some attributes based on these population distributions.

Following the population of the home regions, the AceMod simulator assigns work and school regions to individuals within the population. This process is based on the "Travel to work" data published by the ABS, which defines a number of individuals N living in home region i and working in region j. In order to satisfy each of these "worker flows", a number of unassigned working-age individuals (19-64 years old) in region i are selected at random and assigned to work in location j. School allocation, on the other hand, is somewhat more complicated as detailed data about student home locations is not available from the ABS. Instead, we use the available data from the Australian Curriculum, Assessment and Reporting Authority (ACARA), detailing the locations of schools, along with a proximity based model which biases children allocation towards closer schools. More detail about student allocation can be found in previous studies [14].

We trace scenarios of COVID-19 pandemic spread in Australia, initiated by passenger arrivals via air traffic from overseas. This process maintains a stream of new infections at each time step, set in proportion to the average daily number of incoming passengers at that airport [14, 15]. These infections occur probabilistically, generated by binomial distribution $B(P, N)$, where P and N are selected to generate one new infection within a 50 km radius of the airport, per 0.04% of incoming arrivals on average.

F. Comparison of parent commitment levels during school closures

Here we compare effects of school closures, added to the case isolation and home quarantine, for two levels of parents' commitment to stay home: 25% and 50%. That is, the proportion of children supervised at home during school closure by one of their randomly chosen parents varies from 25% to 50%, as shown by Fig. 11. Focussing on the 25% commitment, we also trace the effects of school closures for two specific age groups: children and individuals over 65 years old, shown in Fig. 12 and 13 respectvely.

G. A delayed introduction of strong social distancing measures

On 21 March 2020, the number of confirmed COVID-19 cases in Australia crossed 1,000. This coincided with the ban on all international arrivals of non-residents, non-Australian citizens, put in place the night
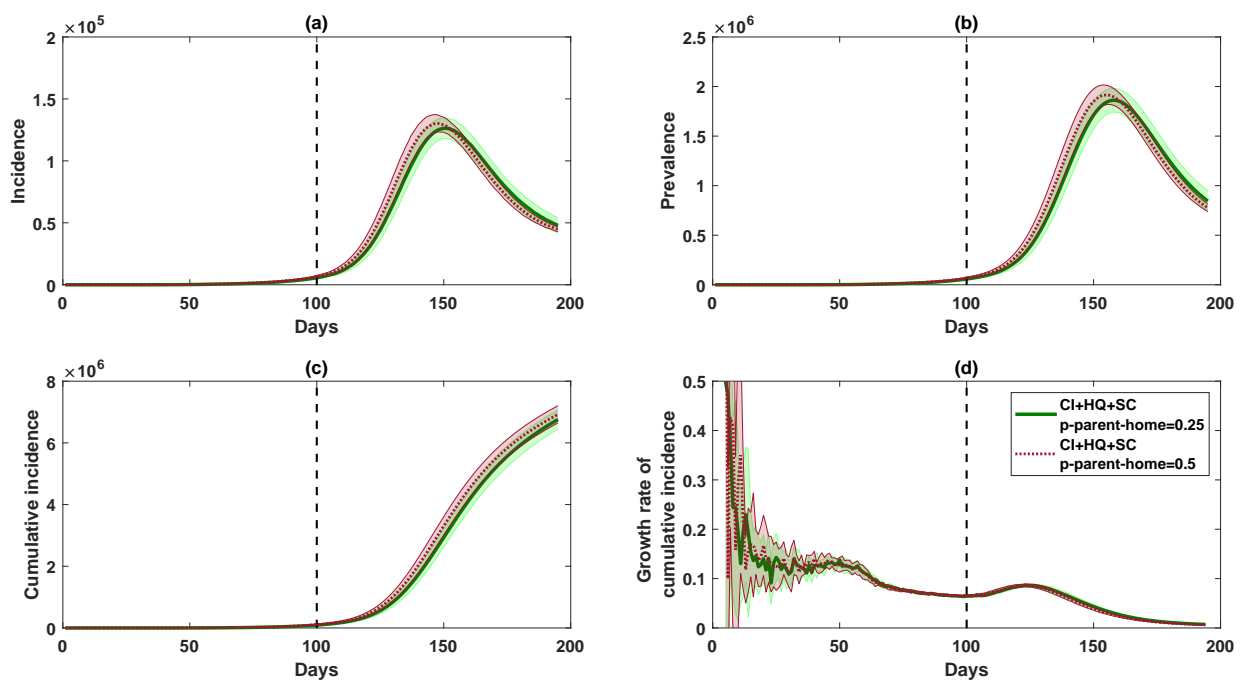
Figure 11: Increasing parents' commitment to stay home during school closures (SC) from 25% (solid) to 50% (dashed) does not significantly affect the spread: incidence (a), prevalence (b), cumulative incidence (c), growth rate of cumulative incidence (d), shown as average (solid) and standard deviation (shaded) profiles, over 10 runs. The strategy with school closures (SC) combined with case isolation and home quarantine lasts 49 days (7 weeks), marked by a vertical dashed line. Restrictions on international arrivals are set to last until the end of each scenario.
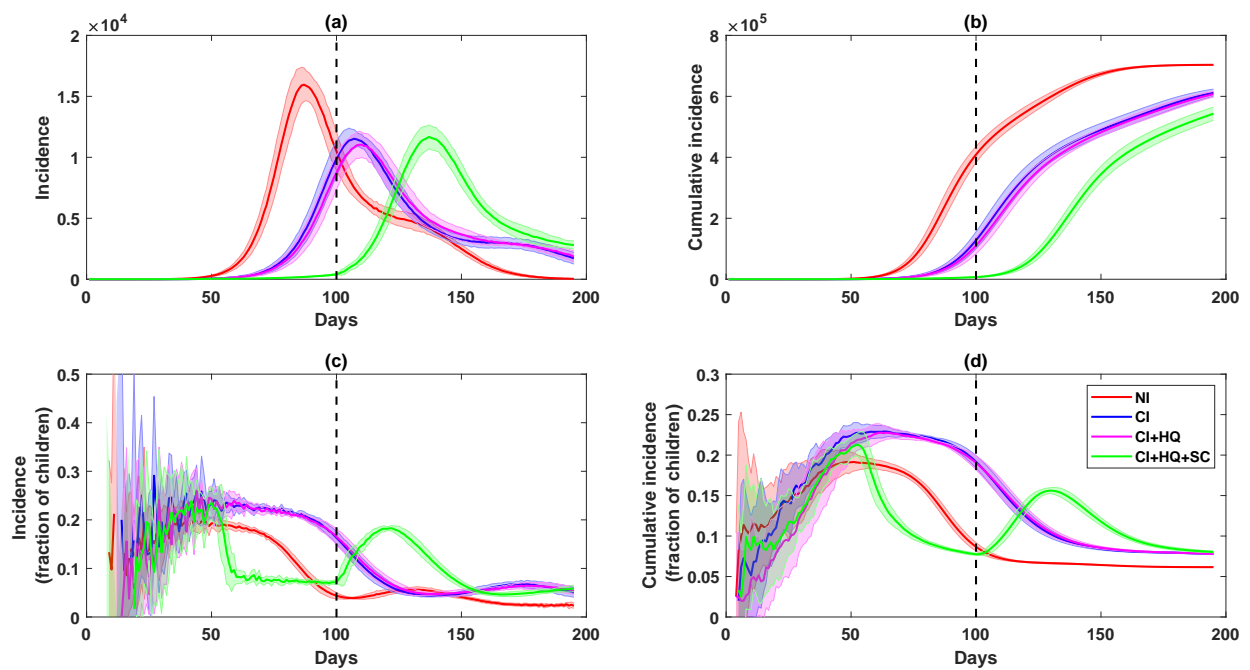
Figure 12: School closures delay incidence peak by four weeks, but increase the fraction of new cases in children around the peak time by 7%. Epidemic curves for children: incidence (a), cumulative incidence (b), fraction of children in incidence (c), and fraction of children in cumulative incidence (d), shown as average (solid) and standard deviation (shaded) profiles, over 10 runs. The strategy with school closures (SC) combined with case isolation and home quarantine lasts 49 days (7 weeks), marked by a vertical dashed line. Restrictions on international arrivals are set to last until the end of each scenario.
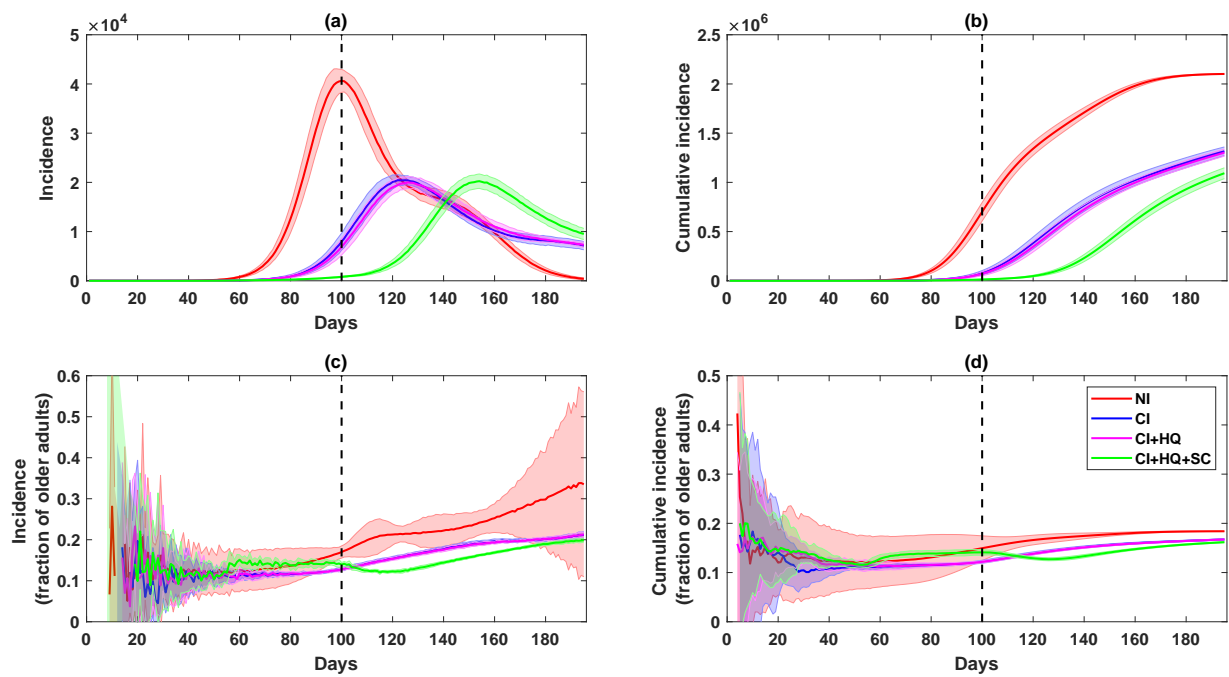
23

Figure 13: School closures delay incidence peak by four weeks, but do not affect new cases for older adults. Epidemic curves for older adults: incidence (a), cumulative incidence (b), fraction of older adults in incidence (c), and fraction of older adults in cumulative incidence (d), shown as average (solid) and standard deviation (shaded) profiles, over 10 runs. The strategy with school closures (SC) combined with case isolation and home quarantine lasts 49 days (7 weeks), marked by a vertical dashed line. Restrictions on international arrivals are set to last until the end of each scenario.

before. The primary scenario considered in this study introduces a social distancing policy, at varying degrees of compliance, triggered by crossing the threshold of 2,000 confirmed cases, exceeded in Australia three days later, on 24 March 2020, when strong measures (e.g., closures of non-essential services and places of social gathering) have been introduced. The primary scenario traced at 90% SD, coupled with case isolation and home quarantine, is well-aligned with the actual epidemic timeline in Australia, as shown in Fig. 14. To re-iterate, the model was calibrated by 24 March 2020, and the comparison across SD levels points to 90% SD as the closest match, but does not change the model parametrization, highlighting its robustness and predictive power.
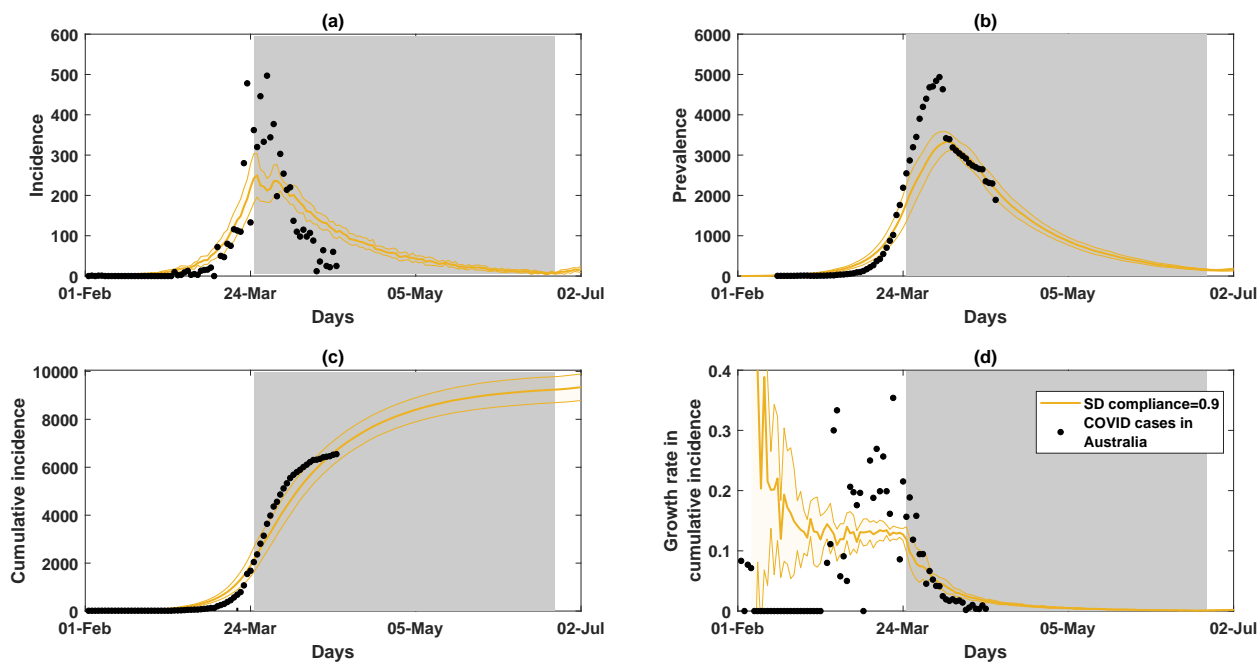

Figure 14: A comparison between actual epidemic curves in Australia (black dots, shown until 19 April 2020), and the primary simulation scenario, using a threshold of 2,000 cases (crossed on 24 March 2020) and following 90% of social distancing (SD), coupled with case isolation and home quarantine (yellow colour), shown until early July 2020. Duration of the SD strategy is set to 91 days (13 weeks), shown as a grey shaded area. Case isolation, home quarantine, and restrictions on international arrivals are set to last until the end of the scenario. Traces include incidence (a), prevalence (b), cumulative incidence (c), and growth rate of cumulative incidence (d), shown as average (solid) and standard deviation (shaded) profiles, over 10 runs. Data sources: [64, 7].

To evaluate a delayed introduction of strong social distancing measures, we compare these two thresholds, separated by three days, while keeping all other parameters unchanged. Referring to Fig. 15, a delayed response results in higher epidemic peaks, doubling the prevalence in comparison with the alternative scenario — across different levels of compliance. The cumulative incidence for 90% SD nearly doubles as well, from around 5,000 total cases, to about 9,000. In the simulation timeline, the threshold of 2,000 cases is crossed on day 50, and if this is aligned with 24 March 2020 on the actual timeline, one may see that the incidence along the 90% SD curve starts to reduce from day 59 (aligned with early April 2020), and the prevalence peak is reached around days 62–65 (aligned with 5–8 April 2020).

This model has been used in Australia in a now-casting mode during the period since 24 March 2020. The early projections of the timing of actual incidence and prevalence peaks, as well as the estimation of the cumulative incidence in Australia to approach the range of 8,000–10,000 total cases, have shown a good accuracy, validating the model. Specifically, the agreement between the actual and simulation timelines appears to be the strongest for 90% SD compliance, applied from 24 March 2020 (i.e., primary scenario with 2,000 cases), following a period of weaker compliance between 21 and 24 of March 2020.

Significant levels of compliance have been also confirmed by the Citymapper Mobility Index, which

collates the usage of the Citymapper app for planning public transport, walking, cycling, and micromobility data [69]. These data allow for approximating the extent of social distancing compliance, showing, by the 26th March 2020, a reduction of 80% from the normal mobility levels for both Sydney and Melbourne. There was a relatively steep drop in mobility to this level, noting that the number of trips taken by residents of Sydney and Melbourne was around 50% just five days prior. Since this drop to now, the levels of compliance have remained relatively constant at 80–90%, peaking at 90% for both Sydney and Melbourne on the 10th April 2020. We point out that in Australia, the healthcare sector alone comprises about 6% the population, with accommodation and food services reaching up to 3.6%, while transport, postal and warehousing sector occupies 2.6%, and electricity, gas, water and Waste services add another 0.6% [70]. Thus, assuming that a substantial fraction of employees delivering these essential services cannot work from home, the highest level of social distance compliance would not exceed 90%.

We also observe that a three-day delay in introducing strong social distancing measures results in an approximately four-week lengthening of the required suppression period, confirmed by separate runs with a longer suppression duration (Table 3). The resultant difference (i.e., delay) averages in 27.14 days, with standard deviation of the difference estimated as 12.238 days.
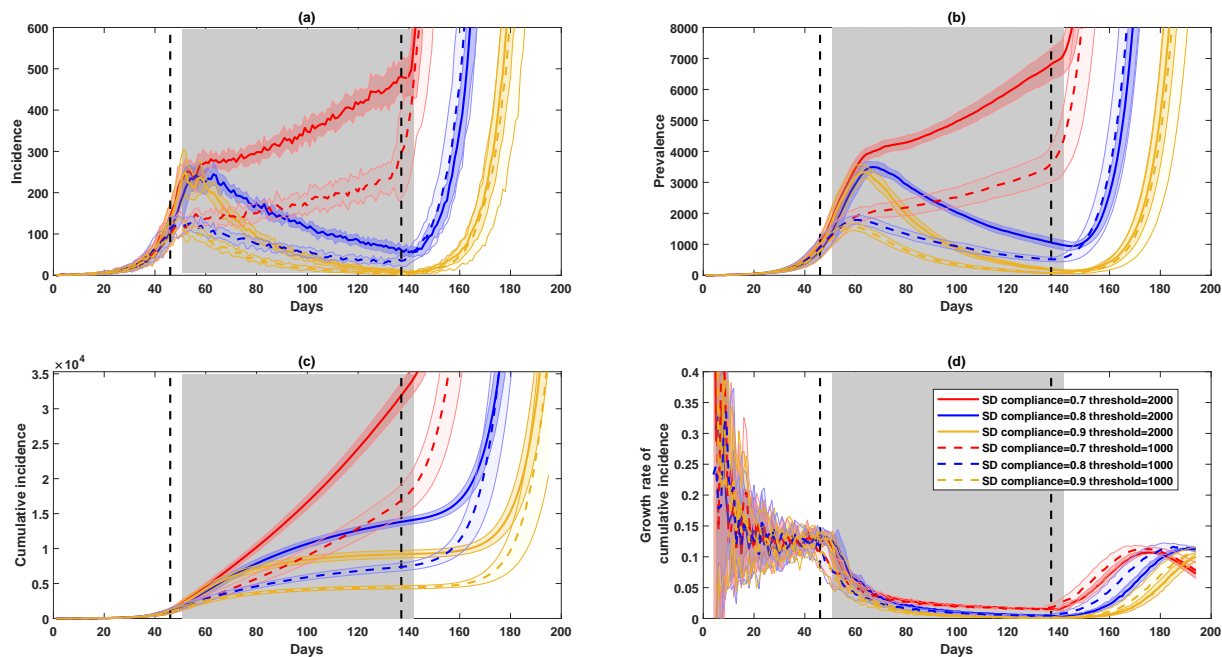

Figure 15: A three-day delay in introducing strict social distancing doubles the disease prevalence. A comparison of social distancing (SD) strategies, coupled with case isolation and home quarantine, across different compliance levels (70%, 80% and 90%). Two scenarios are contrasted: primary scenario with the threshold set at 2,000 cases (matching actual numbers on 24 March 2020), and the alternative threshold of 1,000 (matching actual numbers on 21 March 2020). Duration of each SD strategy is set to 91 days (13 weeks), shown as a grey shaded area for the primary threshold (2,000 cases), and with vertical dashed lines for the alternative threshold (1,000 cases). Case isolation, home quarantine, and restrictions on international arrivals are set to last until the end of each scenario. Traces include incidence (a), prevalence (b), cumulative incidence (c), and the growth rate of cumulative incidence $\dot{C}$ (d), shown as average (solid) and standard deviation (shaded) profiles, over 10 runs.

Table 3: The average differences between early and delayed interventions. A comparison between two scenarios: early interventions (threshold 1,000 cases) and delayed interventions (threshold 2,000 cases). Each scenario is evaluated over 10 runs. In each run, a day is recorded when the prevalence decreases below a specified criterion in terms of active cases (ranging from 30 to 50 in increments of 5).

Criterion	Threshold 1,000		Threshold 2,000		Difference	
(prevalence)	(day)	(std. dev.)	(day)	(std. dev.)	(days)	(std. dev.)
50	146.8	7.756	173.8	7.547	27.0	10.822
45	150.2	9.662	177.2	7.153	27.0	12.022
40	152.0	10.286	179.7	7.267	27.7	12.594
35	155.5	10.819	184.9	7.148	29.4	12.967
30	160.4	11.543	185.0	5.500	24.6	12.786
Average					27.14	12.238

Table 4: Average fractions of local transmission (over 10 runs), in %. NI: no intervention, CI: case isolation, HQ: home quarantine, SC: school closures, SD: social distancing. For NI, CI, HQ and SC: shown at the end of suppression of SC, i.e., after 49 days. For SD: shown at the end of suppression of SD, i.e., after 91 days. The contexts include households (HH), household clusters (HC), census districts (CD), statistical areas (SA2), working groups (WG), classrooms (CL), grades (GR), schools (SCH).

Scenario	HH	HC	CD	SA2	WG	CL	GR	SCH
NI	17.83700	17.20191	25.83878	13.93359	20.46721	1.909873	1.437532	1.374105
CI	28.30946	15.02627	17.16258	9.396544	17.36988	5.082292	3.897974	3.755020
CI+HQ	30.43771	14.29693	16.60576	9.123177	17.03135	4.990329	3.830796	3.683965
CI+HQ+SC	26.75985	17.07578	25.48842	14.10395	16.20378	0.144116	0.113167	0.110907
CI+HQ+SD 10%	30.65391	14.88000	20.79729	11.32239	16.52561	2.348359	1.783789	1.688453
CI+HQ+SD 20%	32.59323	14.78506	20.17335	11.00841	15.18771	2.512762	1.917718	1.821719
CI+HQ+SD 30%	34.64742	14.60785	19.25648	10.51876	13.80992	2.867991	2.197846	2.093714
CI+HQ+SD 40%	36.63812	14.34606	18.31328	10.01645	12.56892	3.219819	2.505355	2.392001
CI+HQ+SD 50%	38.45616	14.21284	17.88055	9.820673	11.33314	3.279559	2.546214	2.470889
CI+HQ+SD 60%	40.49414	14.11064	18.13496	9.954394	9.831069	2.916156	2.310511	2.248137
CI+HQ+SD 70%	42.53621	14.08557	18.98332	10.35789	8.160545	2.306105	1.815167	1.755184
CI+HQ+SD 80%	44.41222	13.83213	18.99710	10.54947	7.081500	1.999026	1.571632	1.556918
CI+HQ+SD 90%	46.20084	13.26401	18.26556	9.995014	6.756665	2.100200	1.733860	1.683832
CI+HQ+SD 100%	47.64493	12.79076	17.03895	9.365276	7.041982	2.424874	1.912616	1.780615

H. Comparison of SD compliance levels across several state capitals

Differences between 70% and 90% SD compliance levels are visualised in choropleth maps of four largest Australian Capital Cities: Sydney, Melbourne, Brisbane and Perth (Fig. 16). These snapshots depict the incidence in these cities at day 60, illustrating how these two compliance levels diverge at that time.

I. Fractions of transmission across mixing contexts

Table 4 summarises fractions of local transmission for the considered scenarios, across mixing contexts: households (HH), household clusters (HC), census districts (CD), statistical areas (SA2), working groups (WG), classrooms (CL), grades (GR), schools (SCH).

Competing interests

Authors declare no competing interests.

Author contributions

References

[1] National Health Commission (NHC) of the People's Republic of China. NHC daily reports (2020). `http://www.nhc.gov.cn/yjb/pzhgli/new_list.shtml`. [Online; accessed 21-March-2020].

[2] Wang, C., Horby, P. W., Hayden, F. G. & Gao, G. F. A novel coronavirus outbreak of global health concern. *The Lancet* **395**, 470–473 (2020).

[3] Report of the WHO–China joint mission on coronavirus disease 2019 (COVID-19). `https://www.who.int/docs/default-source/coronaviruse/who-china-joint-mission-on-covid-19-final-report.pdf` (2020).

[4] Vital surveillances: The epidemiological characteristics of an outbreak of 2019 novel coronavirus diseases (COVID-19)–China, 2020. the novel coronavirus pneumonia emergency response epidemiology team. *China CDC Weekly* **2**, 113–122 (2020).

[5] WHO Director-General's opening remarks at the media briefing on COVID-19 – 11 March 2020 (2020). `https://www.who.int/dg/speeches/detail/who-director-general-s-opening-remarks-at-the-media-briefing-on-covid-19---11-march-2020`. [Online; accessed 21-March-2020].

[6] Dong, E., Du, H. & Gardner, L. An interactive web-based dashboard to track COVID-19 in real time. *The Lancet Infectious Diseases* (2020).

[7] Coronavirus COVID-19 global cases: Johns Hopkins University. `https://www.arcgis.com/apps/opsdashboard/index.html` (2020).

[8] Longini, I. M. *et al.* Containing pandemic influenza at the source. *Science (New York, N.Y.)* **309**, 1083–1087 (2005).

[9] Ferguson, N. M. *et al.* Strategies for containing an emerging influenza pandemic in Southeast Asia. *Nature* **437**, 209–214 (2005).

[10] Nsoesie, E. O., Beckman, R. J. & Marathe, M. V. Sensitivity analysis of an individual-based model for simulation of influenza epidemics. *PLOS ONE* **7**, 0045414 (2012).

[11] Nsoesie, E. O., Brownstein, J. S., Ramakrishnan, N. & Marathe, M. V. A systematic review of studies on forecasting the dynamics of influenza outbreaks. *Influenza and other respiratory viruses* **8**, 309–316 (2014).

[12] Herron, J. & Hajric, V. 'The Market's in Panic Mode.' Stock Markets Plunge 12% Amid Coronavirus Fears (2020). `https://time.com/5803847/coronavirus-stocks-fall/`. [Online; accessed 21-March-2020].

[13] Ferguson, N. M. *et al.* Impact of non-pharmaceutical interventions (NPIs) to reduce COVID-19 mortality and healthcare demand. *Preprint, Imperial College COVID-19 Response Team* (2020).

[14] Zachreson, C. *et al.* Urbanization affects peak timing, prevalence, and bimodality of influenza pandemics in Australia: results of a census-calibrated model. *Science Advances* **4**, eaau5294 (2018).

[15] Harding, N., Spinney, R. E. & Prokopenko, M. Phase transitions in spatial connectivity during influenza pandemics. *Entropy* **22**, 133 (2020).

[16] Zachreson, C., Fair, K. M., Harding, N. & Prokopenko, M. Interfering with influenza: nonlinear coupling of reactive and static mitigation strategies. *Journal of The Royal Society Interface* **17**, 20190728 (2020).

[17] Cauchemez, S. *et al.* Role of social networks in shaping disease transmission during a community outbreak of 2009 H1N1 pandemic influenza. *Proceedings of the National Academy of Sciences* **108**, 2825–2830 (2011).

[18] Cliff, O. M. *et al.* Investigating spatiotemporal dynamics and synchrony of influenza epidemics in Australia: an agent-based modelling approach. *Simulation Modelling Practice and Theory* **87**, 412–431 (2018).

[19] Halloran, M. E., Longini, I. M., Nizam, A. & Yang, Y. Containing bioterrorist smallpox. *Science* **298**, 1428–1432 (2002).

[20] Eubank, S. *et al.* Modelling disease outbreaks in realistic urban social networks. *Nature* **429**, 180 (2004).

[21] Longini, I. M., Halloran, M. E., Nizam, A. & Yang, Y. Containing pandemic influenza with antiviral agents. *American Journal of Epidemiology* **159**, 623–633 (2004).

[22] Germann, T. C., Kadau, K., Longini, I. M. & Macken, C. A. Mitigation strategies for pandemic influenza in the United States. *Proceedings of the National Academy of Sciences* **103**, 5935–5940 (2006).

[23] Barrett, C., Bisset, K., Leidig, J., Marathe, A. & Marathe, M. V. An integrated modeling environment to study the co-evolution of networks, individual behavior and epidemics. *AI Magazine* **31**, 75–87 (2010).

[24] Balcan, D. *et al.* Modeling the spatial spread of infectious diseases: The global epidemic and mobility computational model. *Journal of Computational Science* **1**, 132–145 (2010).

[25] Chao, D. L., Halloran, M. E., Obenchain, V. J. & Longini Jr, I. M. FluTE, a publicly available stochastic influenza epidemic simulation model. *PLoS Computational Biology* **6**, e1000656 (2010).

[26] Bisset, K. R. *et al.* Simulating the spread of infectious disease over large realistic social networks using charm++. In *Parallel and Distributed Processing Symposium Workshops & PhD Forum (IPDPSW), 2012 IEEE 26th International*, 507–518 (IEEE, 2012).

[27] Moss, R. *et al.* Modelling the impact of COVID-19 in Australia to inform transmission reducing measures and health system preparedness. *medRxiv* (2020).

[28] Harding, N., Nigmatullin, R. & Prokopenko, M. Thermodynamic efficiency of contagions: a statistical mechanical analysis of the SIS epidemic model. *Interface Focus* **8**, 20180036 (2018).

[29] Harding, N., Spinney, R. E. & Prokopenko, M. Population mobility induced phase separation in SIS epidemic and social dynamics. *Scientific Reports, in press* (2020).

[30] Drossel, B. & Schwabl, F. Forest-fire model with immune trees. *Physica A: Statistical Mechanics and its Applications* **199**, 183–197 (1993).

[31] Clar, S., Schenk, K. & Schwabl, F. Phase transitions in a forest-fire model. *Physical Review E* **55**, 2174–2183 (1997).

[32] Guisoni, N., Loscar, E. & Albano, E. Phase diagram and critical behavior of a forest-fire model in a gradient of immunity. *Physical Review E* **83**, 011125 (2011).

[33] Antia, R., Regoes, R. R., Koella, J. C. & Bergstrom, C. T. The role of evolution in the emergence of infectious diseases. *Nature* **426**, 658–661 (2003).

[34] Erten, E., Lizier, J., Piraveenan, M. & Prokopenko, M. Criticality and information dynamics in epidemiological models. *Entropy* **19**, 194 (2017).

[35] Dehning, J. *et al.* Inferring COVID-19 spreading rates and potential change points for case number forecasts. *arXiv preprint arXiv:2004.01105* (2020).

[36] Gemeinholzer, B. Phylogenetic networks. *Analysis of biological networks* 255–282 (2008).

[37] Piraveenan, M., Prokopenko, M. & Zomaya, A. Y. Assortativeness and information in scale-free networks. *European Physical Journal B* **67**, 291–300 (2009).

[38] Junker, B. H. & Schreiber, F. *Analysis of biological networks*, vol. 2 (John Wiley & Sons, 2011).

[39] Piraveenan, M., Prokopenko, M. & Zomaya, A. Y. Assortative mixing in directed biological networks. *IEEE/ACM Transactions on Computational Biology and Bioinformatics* **9**, 66–78 (2012).

[40] Cliff, O. *et al.* Network properties of Salmonella epidemics. *Scientific Reports* **9**, 6159 (2019).

[41] Marais, B. J. *et al.* Improving emergency preparedness and response in the Asia-Pacific. *BMJ Global Health* **4**, e001271 (2019).

[42] Chang, S. L., Piraveenan, M. & Prokopenko, M. The effects of imitation dynamics on vaccination behaviours in SIR-network model. *International Journal of Environmental Research and Public Health* **16**, 2477 (2019).

[43] Chang, S. L., Piraveenan, M., Pattison, P. & Prokopenko, M. Game theoretic modelling of infectious disease dynamics and intervention methods: a review. *Journal of Biological Dynamics* **14**, 57–89 (2020).

[44] Gros, C., Valenti, R., Schneider, L., Valenti, K. & Gros, D. Containment efficiency and control strategies for the corona pandemic costs. *arXiv preprint arXiv:2004.00493* (2020).

[45] Vattay, G. Predicting the ultimate outcome of the COVID-19 outbreak in Italy. *arXiv preprint arXiv:2003.07912* (2020).

[46] Walker, P. G. T. *et al.* The global impact of COVID-19 and strategies for mitigation and suppression. *Preprint, Imperial College COVID-19 Response Team* (2020).

[47] Dignum, F. *et al.* Agent-based social simulation for the analysis of social, health and economic effects of the coronavirus pandemic - conceptual model. Accessed: 01-04-2020.

[48] Fair, K. M., Zachreson, C. & Prokopenko, M. Creating a surrogate commuter network from Australian Bureau of Statistics census data. *Scientific data* **6**, 150 (2019).

[49] Carrat, F. *et al.* Time lines of infection and disease in human influenza: a review of volunteer challenge studies. *American Journal of Epidemiology* **167**, 775–785 (2008).

[50] Leung, N. H., Xu, C., Ip, D. K. & Cowling, B. J. The fraction of influenza virus infections that are asymptomatic: a systematic review and meta-analysis. *Epidemiology (Cambridge, Mass.)* **26**, 862 (2015).

[51] Guan, W.-j. *et al.* Clinical characteristics of coronavirus disease 2019 in China. *New England Journal of Medicine* (2020).

[52] Li, R. *et al.* Substantial undocumented infection facilitates the rapid dissemination of novel coronavirus (SARS-CoV2). *Science* (2020).

[53] Kucharski, A. J. *et al.* Early dynamics of transmission and control of COVID-19: a mathematical modelling study. *The Lancet Infectious Diseases* (2020).

[54] Li, Q. *et al.* Early transmission dynamics in Wuhan, China, of novel coronavirus–infected pneumonia. *New England Journal of Medicine* (2020).

[55] Linton, N. M. *et al.* Incubation period and other epidemiological characteristics of 2019 novel coronavirus infections with right truncation: a statistical analysis of publicly available case data. *Journal of Clinical Medicine* **9**, 538 (2020).

[56] Mizumoto, K., Omori, R. & Nishiura, H. Age specificity of cases and attack rate of novel coronavirus disease (COVID-19). *medRxiv* (2020).

[57] Huang, H. *et al.* Epidemic features and control of 2019 novel coronavirus pneumonia in Wenzhou, China. *Preprints with The Lancet* (2020).

[58] Nishiura, H. *et al.* Estimation of the asymptomatic ratio of novel coronavirus infections (covid-19). *medRxiv* (2020).

[59] Mizumoto, K., Kagaya, K., Zarebski, A. & Chowell, G. Estimating the asymptomatic proportion of coronavirus disease 2019 (covid-19) cases on board the diamond princess cruise ship, yokohama, japan, 2020. *Eurosurveillance* **25**, 2000180 (2020).

[60] Bi, Q. *et al.* Epidemiology and transmission of COVID-19 in Shenzhen China: Analysis of 391 cases and 1,286 of their close contacts. *medRxiv* (2020).

[61] Dong, Y. *et al.* Epidemiological characteristics of 2143 pediatric patients with 2019 coronavirus disease in China. *Pediatrics* (2020).

[62] Wikipedia contributors. 201920 coronavirus pandemic in mainland China — Wikipedia, The Free Encyclopedia (2020). https://en.wikipedia.org/wiki/201920_coronavirus_pandemic_in_mainland_China. [Online; accessed 24-March-2020].

[63] Wikipedia contributors. 2020 coronavirus pandemic in <nation> — Wikipedia, The Free Encyclopedia (2020). [Online;

accessed 24-March-2020; nation: France; Germany; Iran; Italy; South Korea; Spain; the United States].

[64] Wikipedia contributors. 2020 coronavirus pandemic in australia — Wikipedia, The Free Encyclopedia (2020). `https://en.wikipedia.org/wiki/2020_coronavirus_pandemic_in_Australia`. [Online; accessed 24-March-2020].

[65] Halloran, M. E. *et al.* Modeling targeted layered containment of an influenza pandemic in the United States. *Proceedings of the National Academy of Sciences* **105**, 4639–4644 (2008).

[66] Mossong, J. *et al.* Social contacts and mixing patterns relevant to the spread of infectious diseases. *PLoS medicine* **5**, e74 (2008).

[67] Miller, J. C. Spread of infectious disease through clustered populations. *Journal of the Royal Society Interface* **6**, 1121–1134 (2009).

[68] Australian Statistical Geography Standard. `https://www.abs.gov.au/ausstats/abs@.nsf/Lookup/2901.0Chapter23102011`. Accessed: 08-10-2019.

[69] CityMapper. CityMapper Mobility Index. `https://citymapper.com/cmi/`. Accessed: 12-04-2020.

[70] Vandenbroek, P. Snapshot of employment by industry, 2019. `https://www.aph.gov.au/About_Parliament/Parliamentary_Departments/Parliamentary_Library/FlagPost/2019/April/Employment-by-industry-2019`. Accessed: 02-04-2020.
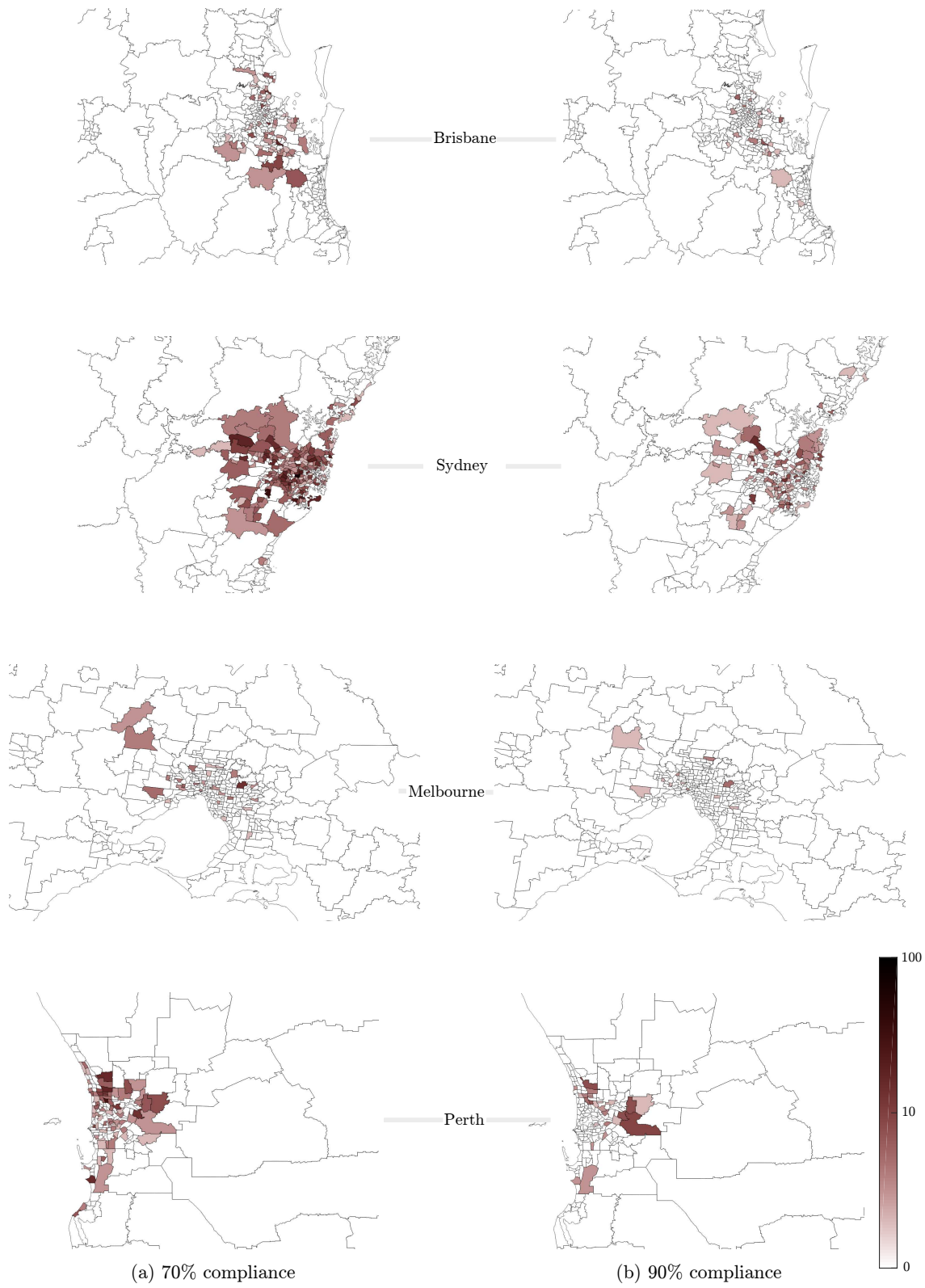
Figure 16: Choropleths of four largest Australian Capital Cities: prevalence on a log scale at day 60.